Marine Pollution Bulletin
July 2021, Volume 168 Pages 112387 (12p.)
https://doi.org/10.1016/j.marpolbul.2021.112387
https://archimer.ifremer.fr/doc/00690/80239/

Coupling high frequency monitoring and bioassay experiments to investigate a harmful algal bloom in the Bay of Seine (French-English Channel)

Serre-Fredj Léon [1, 2], Jacqueline Franck [3], Navon Maxime [1, 2], Izabel Guillaume [1, 4], Chasselin Leo [1, 4], Jolly Orianne [1, 4], Repecaud Michel [5], Claquin Pascal [1, 2, *]

[1] Normandie Université, Université de Caen Normandie, Esplanade de la Paix, F-14032, Caen, France
[2] Laboratoire Biologie des ORganismes et Ecosystèmes Aquatiques (BOREA, UMR 8067), Sorbonne Université, Muséum National d'Histoire Naturelle, CNRS, Université Pierre et Marie Curie, Université de Caen Normandie, IRD 207, Université des Antilles. Centre de Recherches en Environnement Côtier (CREC), Station Marine, BP49, 54, rue du Docteur Charcot, 14530 Luc-sur-Mer, France
[3] Ifremer LER/N, Avenue du Général de Gaulle, 14520 Port-en-Bessin, France
[4] Centre de Recherches en Environnement Côtier (CREC) - Station Marine de l'Université de Caen Normandie, BP49, 54, rue du Docteur Charcot, 14530, France
[5] Ifremer Centre de Brest REM/RDT/DCM, ZI de la pointe du Diable CS 10070, 29280 Plouzané, France

* Corresponding author : Léon Serre-Fredj, email address : pascal.claquin@unicaen.fr

Abstract :

Coastal ecosystems are increasingly threatened by eutrophication and dystrophy. In this context, the full pattern of a bloom dominated by the dinoflagellate, Lepidodinium chlorophorum, was investigated by a high frequency monitoring buoy equipped with sensors allowing nutrients and photosynthesis measurements. An increase of the N/P ratio affected phytoplankton physiology leading to bloom collapse with a slight oxygen depletion. In parallel, enrichment experiments were performed on the natural bloom population. After 5 days of incubation the community structure, using flow cytometry and several physiological parameters were analysed. The data reveal a potential N and P co-limitation and a decoupling between primary production and productivity in fully enriched conditions. Under unbalanced N/P inputs, high level of alkaline phosphatase activity and transparent exopolymeric particle production, which favour phytoplankton sedimentation, were observed. Nutrient inputs and their stoichiometry control phytoplankton growth, the community structure, physiological regulations, the fate of the bloom and consequences.

Graphical abstract

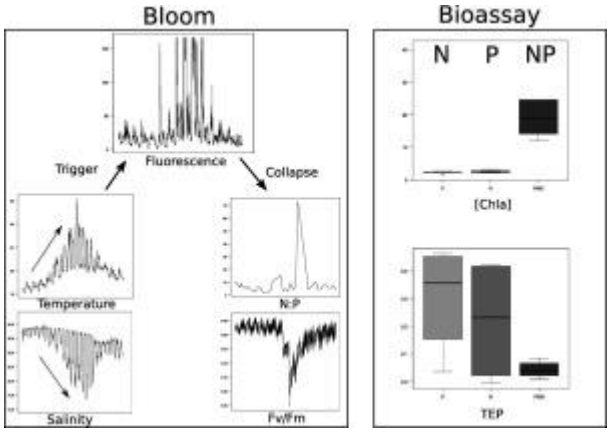

Highlights

► *Lepidodinium chlorophorum* harmfull algal bloom fully monitored at high frequency ► Triggering and fate of the bloom explore with nutrients and photosynthetic HF data ► P limitation cause the bloom decline as flagged by the Fv/Fm and N/P ratio. ► Enrichment experiment reveal potential N and P co limitation. ► High TEP production under N or P limitation in enrichment experiment

Keywords : Lepidodinium chlorophorum, Eutrophication, FRRf, Transparent exopolymeric particles, Flow cytometry

1. Introduction

As the ocean's first frontier, coastal ecosystems are increasingly under threats that affect many essential benthic and pelagic habitats of marine species (Barbier et al., 2011). Eutrophication, which is due to excess nutrient inputs in coastal systems caused by human activities is one of the major environmental problems affecting coastal ecosystem in the world (Rabalais et al., 2009). These inputs affect both the concentration of nutrients and their stoichiometry (Martin et al., 2008; Watanabe et al., 2017). The growth and diversity of primary producers, like phytoplankton, which are at the base of the marine food web, are largely controlled by these inputs (Smith, 2006). Unbalanced nutrient inputs and dystrophy, both frequently linked with eutrophication, have several effects on phytoplankton: modification of communities (Leruste et al., 2019; Shen, 2001), alter the growth rate (Nwankwegu et al., 2020), produce allochemical-like toxins which, in turn, favour monospecific blooms (Granéli et al., 2008). Associated with other environmental parameters including light, temperature, water mass resistance time, or river discharges, nutrient inputs can lead to phytoplankton blooms (Heisler et al., 2008) that may be classified as harmful algal blooms (HAB) (Anderson, 2009). HAB species are usually split into two groups, one of which is able to produce toxins or harmful metabolites that damage wildlife, or result in poisoning of human seafood, and the second in which high densities of non-toxic cells can harm the environment by producing scums or foams which lead to oxygen depletion (Anderson et al., 2002).

Nutrient inputs into the Bay of Seine (France) are mainly controlled by inputs from the Seine River (Aminot et al., 1998) although smaller rivers inputs also have local impacts (Lemesle et al., 2015). Over the last decades, many programmes for the management of nutrient inputs have reduced nutrient discharges but have mainly had an impact on phosphorus inputs, whereas N inputs remain high (Garnier et al., 2019). The stoichiometry of nutrient inputs have been broadly modified over the last decade and very high N/P ratio inputs are regularly measured in the Seine River and Seine estuary (Meybeck et al., 2018).

Although chlorophyll biomass has decreased in recent years in the English Channel (Gohin et al., 2019), the relative proportion of the dinoflagellate group has increased (Hernández-Fariñas et al., 2014; Widdicombe et al., 2010). In the Bay of Seine, several species of dinoflagellate like *Karenia mikimotoi* and *Lepidodinium chlorophoru*m are able to form large harmful algal bloom (HAB) (Napoléon et al., 2014). *Lepidodinium chlorophoru*m is known to produce large quantities of transparent exopolymeric particles (TEP) (Claquin et al., 2008) and to be responsible for the mortality of marine organisms due to oxygen depletion induced by decomposition of the population (Sournia et al., 1992).

Many studies have shown that phytoplankton communities can respond within a few hours after an environmental change (Lefort and Gasol, 2014; Thyssen et al., 2008) which stresses out the necessity of implementing a high frequency sampling (Bouman et al., 2005). In the present work, a late summer *L. chlorophorum* bloom event was studied in detail using high frequency measurements made by an instrumented buoy called SMILE (0° 19.68', 49° 21.23'). In addition to standard sensors (temperature, salinity, turbidity, oxygen, light and fluorescence), the SMILE buoy is equipped with a fast repetition rate fluorimeter (FRRf), which enables photobiological and physiological measurements of the phytoplankton communities, and two types of nutrient sensors, which together provide new and more realistic pictures of bloom dynamics.

In addition to monitoring the bloom event, enrichment bioassay experiments were performed on samples collected during the bloom in order to understand how nutrient inputs influence the structure and physiological parameters of the communities. The specific objectives of our studies were to:

1) Characterise bloom dynamics from an original point of view by including physiological, productivity, and nutrients measurements at a high frequency.

2) investigate phytoplankton dynamics and the ecophysiology of a community dominated by *L. chlorophorum* as a function of nutrient inputs.

2. Material and Methods

2.1. High frequency measurements using an instrumented buoy

The bloom event was monitored *in situ* using the SMILE buoy in the Bay of Seine (Fig. 1) measuring since 2016 which belong the COAST-HF network (French Coastal ocean observing system - High frequency). Different types of measurements were performed at different frequencies by the buoy.

2.1.1. List of measurements performed at high frequency by the buoy

Conductivity and temperature (tetracon sensor, WTW^{TM}, Germany), turbidity (Seapoint turbidity meter, Seapoint Sensor, USA), oxygen (AADI Oxygen optode, Aanderraa, Norway) and in-vivo fluorescence (Cyclops-6K, Turner Design, USA) sensors that measure fluorescent in fluorescein in fluorescent units (FFU) are grouped in a multiparameter probe NKE instrument (MP7, NKE Instrumentation ®, France), PAR (Photosynthetically active radiation) is measured with a Satlantics sensor (Satlantics, Italy). All these parameters were measured at 20-min intervals (data available doi.org/10.17882/53689). Photosynthetic parameters were determined at 2-h intervals using the FastOcean FRRf3 sensor with the Act2 system (Chelsea Technologies, UK) with an excitation light provided by a blue light-emitting diode (450 nm). Inorganic nutrients (NO_3^-, PO_4^{2-}, NH_3, NO_2^-) were measured by the chemical probe Wiz (SYSTEA S.p.A, Italy) once a day while an optical sensor, OPUS (Trios, Germany), also measured NO_3^- at 20-min intervals. All measurements were performed at one-meter depth.

2.1.2. High-frequency measurements of inorganic nutrients

The Wiz probe uses micro loop flow analysis (µLFA) for autonomous measurements of four nutrients (NO_3^-, PO_4^{2-}, NO_2^-) using colourimetric methods and NH_3 with a fluorimetric method (Azzaro, 2014; Moscetta et al., 2009). As the buoy has limited energy, measurements were only

performed once a day. The detection limits were 0.35 µmol.l^{-1} for NO_3^- and 9.2.10^{-2} µmol.l^{-1} for PO_4^{2-}. NO_3^- was also measured using an optical sensor (OPUS, Trios, Germany). The OPUS UV is a spectral sensor equipped with a xenon flash lamp as light source and a high-end miniature spectrometer (MMS, Zeiss, Germany) with 256 channels covering the spectral range from 200 to 360 nm as detector. This sensor measures NO_3^- at high frequency with low energy consumption. A 20-mm optical path allowed measurements from 1 to 357 µmol.l^{-1} with a precision of 0.18 µmol.l^{-1}.

2.1.3. High frequency photosynthetic measurements

FLCs (fluorescent light curve) were measured *in situ* by the buoy using a FRRf-ACT2. The samples were analysed after a 5 min period of dark incubation for the oxidation of the Quinone A (Q_A). At the end of the dark period F_0 (minimum fluorescence) was measured by using non actinic weak light. A single-turnover (ST) protocol consisting of 100 flashlets of 1 µs with 2 µs of interval was applied for measuring Fm (maximum fluorescence in dark) (Kolber et al. 1998). The maximum quantum efficiency of PSII (F_v/F_m) was calculated as (Genty et al., 1989):

$$\frac{F_v}{F_m} = \frac{(F_m - F_0)}{F_m}$$

Samples were then exposed to 10 light steps of increasing PAR (from 0 to 1,500 µmol photon.s^{-1}.m^{-2}) for 30-sec each step. The effective quantum efficiency of PSII ($F_{q'}/F_{m'}$) was measured at each light step as (Genty et al 1989):

$$\frac{F_{q'}}{F_{m'}} = \frac{(F_{m'} - F')}{F_{m'}}$$

Where $F_{m'}$ is the maximum fluorescence under light and F' the steady state fluorescence under light. The relative electron transport rate (rETR, relative unit) was calculated for each irradiance (E) as:

$$rETR(E) = \frac{F_{q'}}{F_{m'}} \times E$$

The maximum relative electron transport rate ($rETR_{max}$) was estimated by fitting the FLC data to the model of Webb et al. (1974) modified by Boatman et al. (2019) using ACT2RUN (Chelsea Technologies, UK) software to estimate α and E_k with α, the initial slope of the FLC, and E_k the light saturation index:

$$rETR(E) = \alpha \times E_K \times \left(1 - e^{-\frac{E}{E_K}}\right) - \beta \times E_{K\beta} \times (1 - e^{-\frac{E-E_K}{E_{K\beta}}})$$

$rETR_{max}$ is calculated as:

$$rETR_{max} = \alpha \times E_K$$

Using the absorption algorithm of Oxborough et al. (2012), the PSII electrons flux per unit volume is calculated as follows:

$$a_{LHII} = \frac{F_m \times F_0}{F_m - F_0} \times K_a \times 10^{-6}$$

where K_a is an inherent constant of the FRRf. Finally, the PSII flux per unit volume (JV_{IImax}) is calculated as:

$$JV_{IImax} = \frac{a_{LHII} \times rETR_{max} \times 3600}{24 \times 10^3}$$

where JV_{IImax} is expressed in mmol $e^-.m^{-3}.h^{-1}$

The electron transport rate (ETR_{IImax}) is calculated as:

$$ETRII_{max} = \frac{JV_{IImax}}{[chla]}$$

where ETR_{IImax} is expressed in mmol e^-.mg $chla^{-1}.h^{-1}$

2.2. Enrichment experiment

Bioassays were designed to assess the impacts of enrichment on phytoplankton assemblages and on physiological responses. The design was modified from Ly et al. (2014) to fit our specific

requirements. Seawater was sampled on the 29th of August 2019 at the SMILE buoy site during the bloom event. The seawater was filtered just after sampling on a 100-µm mesh to remove grazers. One hour after sampling, enrichments were applied to 500-ml sub-samples in polycarbonate bottles to perform the bioassays. All the bioassays were incubated in a water bath incubator under natural sunlight for 5 days. The water bath incubator was continuously fuelled with seawater pumped directly from the sea to maintain the temperature. The seawater temperature and PAR were recorded at 5-min intervals by respectively, a RBRsolo T logger and a RBR solo^3 PAR logger connected to a Li-COR "Underwater Quantum Sensor" LI-192. Five types of enrichments, each with five replicates, were performed in the incubator: C (control, no enrichment), P (+P), N (+N), NSI (+N+Si) and PNSI (+P+N+Si). The enrichments applied to the bioassays were defined by the maximum value of N, P and Si measured over the year 2018 in the Bay of Seine by the National Network for Environmental Survey SOMLIT (https://www.somlit.fr/ since 2007 at this site) as respectively 50 µmol.l^{-1} for N, 3 µmol.l^{-1} for P and 50 µmol.l^{-1} for Si.

After 5 days, after homogenisation, 25 ml were sampled from all the bioassay bottles to measure phtosynthetic parameters, and phytoplankton functional types and alkaline phosphatase activity (APA). At day 5, supplementary measurements of TEP, nutrients and Chla concentration were performed. Only the data obtained at day 5 are shown here. All the measurements were also made just before enrichment at day 0 (D0).

2.2.1. Photosynthetic measurements

Photosynthetic measurements were performed with a second FRRf-ACT2. The same protocol as the one described above for *in-situ* measurements was applied to the samples for incubation. A 5-ml aliquot of sample was placed in the measuring chamber of the FRRf-ACT2 and FLC were performed after a 5-min period of dark adaption.

2.2.2. Flow cytometry

. Unfixed sample were analysed within one hour of sampling with the CytoSense (Cytobuoy b.v., Netherland) equipped with a blue laser (488 nm, 50 mW) and a green laser (552 nm, 50 mW). This

produces pulse shapes based on the inherent optical properties of the particle when they cross the laser: sideward angle scatter (SWS), forward scatter (FWS), red (FLR, 668-734 nm), orange (FLO, 601-668 nm) and yellow fluorescence (FLY, 536-601 nm). The threshold was set at 16 mV to reduce data acquisition concerning non-photosynthetic particles triggered on FLR, for each sample (5 per enrichment) 380 µl were analysed with a speed of 2.0 $\mu l.s^{-1}$. The CytoSense can analyse chains, cells, or colonies between 1 and 800 µm in diameter, microspheres measuring between 1 µm (Yellow-Green fluorescent, FluoSpheres®) and 1.6 µm (non-fluorescent, provided by Cytobuoy) were used to calibrate size recording (daily use). In order to improve the clustering a mix of bead were analysed with the 1 µm and 1.6 µm and supplementary beads after this experiment (2 µm, 6 µm, 10 µm, 20 µm, Fluoresbrite® YG microsphere, Polyscience) to establish size regression (2-6 µm and 6-20 µm) and discriminate picoeukaryotes, nanoeukaryotes and microphytoplankton. To distinguish the phytoplankton (Fig., 2), five clusters were determined using the cells' optical properties and attributed to *Synechococcus* spp., picoeukaryotes, nanoeukaryotes and microphytoplankton, Cryptophytes and *Lepidodinium chlorophorum* (Elbrächter and Schnepf, 1996; Hansen et al., 2007). The *Synechococcus* spp. cluster has the smallest FWS signal and a high orange fluorescence (FLO) signal which matches very small cells with a high concentration of phycoerythrin.

To accurately define the cytometric signature of *L. chlorophorum*, this species was isolated from the water sample during the bloom event. After a few days in culture, the isolated strains of *L. chlorophorum* were analysed on the CytoSense to match the signature. Picoeukarotic cells are small cells (< 2 µm) and produce low FLR and FWS signals. Nanoeukaryotics and microphytoplankton cells were differentiated from picoeukaryotic cells using the amplitude of the FLR signal and the bead signal. Cryptophyte clusters have higher FLO than *Synechoccocus* due to the high concentrations of phycoerythrin in their cells and an FWS equivalent to the nanoeukaryotic and microphytoplankton cells (Olson et al., 1989; Thyssen et al., 2014).

2.2.3. Measurements of inorganic nutrients (NO_3^-, PO_4^{3-}, $Si(OH)_4$)

Water samples were collected and filtered through a cellulose acetate filter (ClearLine, CA, 33 mm, 0.45 µm) in 50 ml falcon tubes and immediately frozen (-20 °C), with the exception of $Si(OH)_4$ (4 °C). Analyses were conducted using a Seal Analytical AA-3 system (Aminot and Kérouel, 2007). The limits of quantifications were 0.02 µmol.l^{-1} for PO_4^{3-} and 0.05 µmol.l^{-1} for NO_3^-, NO_2^-, $Si(OH)_4$. N/P ratio was calculated as $(NO_2^- + NO_3^-)/ PO_4^{3-}$.

2.2.4. Chlorophyll-a measurements

Water samples (250 ml) were filtered through a glass-fiber filter (Whatman, GF/F, 47 mm) and immediately frozen (-20 °C) until analysis. Ten ml of 90% acetone (v/v) were added to extract the pigment and the samples were then left in the dark at 4 °C for 12 h. After being centrifuged for 5 min at 1,700 g twice, the Chl a concentration of the extracts was measured using a Trilogy fluorimeter (Turner Designs, Sunnyvale, USA) according to the method of Strickland and Parsons (1972).

2.2.5. Transparent exopolymeric particles (TEP)

Water samples (150-200 ml) were filtered through polycarbonate membrane filters (Millipore, 0.4 µm) and immediately frozen (-20 °C) until analysis. According to Claquin et al. (2008) adapted from Passow and Alldredge (1996), the filters were stained with a solution 0.02% Alcian blue (Sigma) with 0.06% acetic acid (pH: 2.5). Excess dye was removed by adding water before centrifugation at 3,000 g, 19 °C for 15 min. This washing cycle was repeated twice, then 6 ml of 80% H_2SO_4 were added. After 2 h, measurements were conducted using a spectrometer (Ultrospec 1000, Pharmacia Biotech) at 787 nm. Calibration were done using a xanthan gum (10-700 µg) as standard, as described by Claquin et al. (2008). After being divided by the Chla concentration, TEP concentrations are expressed in µg Xanthan eq.µg chla^{-1}.

2.2.6. Alkaline phosphatase activity (APA)

APA, as the potential maximum activity per chlorophyll unit,was measured according to Hrustic et al, (2017). Samples (3920-µl) were placed in an UV-cuvette and 80 µl of 4-Methylumbelliferyl phosphatase (MUF-P) 500 µM substrate were added. While incubating at room

temperature, the samples were measured at hourly intervals over a total period of 7 h. Measurements were taken with a RF-6000 spectrofluorophotometer (Shimadzu, Japan). APA was calculated as the slope of the linear regression of the evolution of concentration while incubating. Using a MUF standard curve, the results are expressed in concentration units per hour divided by the concentration in Chl *a* to normalize ($nM.h^{-1}.\mu g\ chla^{-1}.l^{-1}$).

2.3. Statistical and data analysis

Analyses were conducted using R software (R-project, CRAN) version 3.6.1. As the incubation data did not follow a normal law, a Kruskall-Wallis test was performed using "stats" package and a Conover-Iman pairwise test was performed using the "conover.test" package. Only significant tests with a p-value < 0.05 were accepted.

3 Results

3.1. Bloom time series

High frequency measurements provided by the SMILE buoy are presented in Fig.3. An increase in FFU and oxygen saturation on the 24th of August indicated the beginning of the bloom and remained high until the end of the bloom event on the 30th of August, 2019 (Fig. 3 A, B). The highest dissolved O_2 concentration and FFU were measured on the 27th of August with respectively 16.5 mg O_2 .l^{-1} and 165 FFU. This highest value of FFU was also reached the 28th, 29th and 30th August because of a saturation of the FFU sensor. The lowest oxygen concentration ever recorded in 2 years (data available) was measured the 31th August with a value of 5.9 mg.l^{-1}. Based on the variation in O_2 and FFU, the bloom lasted six days. The temperature increased from 19. 3 °C on the 20th of August to reach a maximum of 23.0 °C on the 27th of August and decreased to 19.6 °C on the 3rd of September (Fig. 3 C). This short rise in temperature occurred after a drop in temperature starting on the 27th of August. Turbidity increased on the 27th of August, three days after the beginning of the bloom, to reach 120 NTU before dropping on the 29th of August (Fig. 3 D). Between the 25 and 30th of August, high freshwater input events were observed, leading to a drop in salinity from 33.7 to 31.4 on the 29th of August (Fig. 3 E). The light pattern appeared to be quite stable between days (with a maximum of 1,600 µmol photons.m^{-2}.s^{-1}) with a decrease at mid-bloom (Fig. 3 F).

Nutrients N, P, Si followed the typical summer trend observed at this site in the English Channel (see Data SOMLIT, the French Coastal Monitoring Network; https://www.somlit.fr/ since 2007 at this site) with low stocks of nutrients at the beginning of August followed by nutrient inputs at the end of the month (Napoleon et al., 2012). An increase in PO_4^{3-} and NO_3^- concentrations was observed on the 21st of August just before the bloom began (Fig. 4 B, C, D). After the beginning of the bloom, NH_3 increased from 2.3 µmol.l^{-1} to 5.5 µmol.l^{-1} on the 4th of September (Fig. 4 A). During the bloom, a decrease was observed in the concentration of PO_4^{3-} from $1.7.10^{-1}$ to $0.2.10^{-1}$

µmol.l^{-1} (Fig. 4 D) whereas there was an increase in NO_3^- which reached 1.5 µmol.l^{-1} and increased the N/P ratio to 71 (Fig. 4 E) on the 26th of August. The OPUS sensor enabled nitrate concentrations to be monitored at a higher frequency (20-min intervals) than the WIZ sensor (24-h intervals). Both sensors showed the same general trend for NO_3^- with an increase at the beginning of the bloom event followed by a decrease on the 29th of August (Fig. 4 B, C). The high frequency data provided by the OPUS sensor revealed a dramatic drop in NO_3^- concentrations on the 26th of August, two days after the beginning of the bloom (Fig. 4 C). The concentration on $Si(OH)_4$ on the 30th of August was 13.16 µmol.l^{-1} according to the SOMLIT database and the Si/N and Si/P ratios were respectively 8.7 and 329.0.

Fv/Fm displayed a daily cyclic pattern, the overall decrease of Fv/Fm the first day (from 20th to 26th August) is less than 0.03. Daily variation display more variation than this overall decrease, the mean value for this 6-days period is 0.57 ± 0.01 (n=60). The Fv/Fm dropped on the 26th of August and reached a minimum value of 0.30 on the 28th of August. Finally, Fv/Fm increased to reach a value of 0.55 on the 1st of September (Fig. 5 A). JV_{IImax} showed a daily cycle based on the daily light cycle. JV_{IImax} values showed a steadily rising trend that reached a peak of 89.51 mmol e^-.m^{-3}.h^{-1} on the 28th of August. After this peak, a dramatic drop in JV_{IImax} values was observed. The JV_{IImax} value reached a value of 89.5 mmol e^-.m^{-3}.h^{-1} on the 27th of August (Fig. 5 B). $ETR_{II}max$ values also showed a daily cycle, in which the values increased steadily before a dramatic drop on the 28th of August. The ETR_{IImax} reached a value of 29.4 mmol e^-.mg chla^{-1}.h^{-1} on the 3rd of September (Fig. 5 C).

3.2. Incubation results

During the 5-day incubation period, the mean value of the water temperature was 19.8 °C and the maximum value of the PAR was 2112 µmol photon.m^{-2}.s^{-1} with an overall mean value during daily light periods of 441 µmol photon.m^{-2}.s^{-1}.

The initial inorganic nutrient pool was low in the D0 sample with 3.0 µmol.l^{-1} of nitrate and a phosphate value below the detection limit (< 0.02 µmol.l^{-1}). After incubation, nitrate concentrations in N and NSi enrichments decreased from 53 µmol.l^{-1} (D0 value + enrichment) to 31.5 ± 7.65 µmol.l^{-1} in each enrichment (Fig 6. A), silica was not consumed in the NSi enrichment (mean = 54.28 µmol.l^{-1}) (Fig 6. C). In the P enrichment, the phosphate concentration decreased from 3 µmol.l^{-1} (D0 value + enrichment) to 1.9 ± 0.15 µmol.l^{-1} (Fig 6. D). Finally, in the NPSi enrichment, both nitrate and phosphate were nearly fully consumed with 3 ± 0.07 µmol.l^{-1} of nitrate and 0.09 ± 0.05 µmol.l^{-1} of phosphate left while only 19 ± 2.14 µmol.l^{-1} of silica remained at the end of the incubation period. After 5 days of incubation, the concentration of Chl *a* decreased in the control, P, N, and NSi enrichments compared to the D0 value of 8.51 ± 1.04 (n=3) whereas in the NPSi Chl *a* concentration (Fig. 7 A) increased significantly (mean = 22.16 µg.l^{-1},Kruskall-Wallis: $\chi^2 = 13.6$; $p_{value} = 8.6.10^{-3}$, Conover: mean $p_{value} = 1.9\ 10^{-3}$).

Some common patterns regarding cells concentration were observed in the cytometric phytoplankton groups in all bioassays with enrichment. In the group of smaller cells: *Synechoccocus*, the number of cells dropped after 5 days of incubation with no significant difference between enrichments (Fig. 7 B). Regarding picoeukaryotes, the mean concentration of cell in the P enrichment ($2.0.10^4 \pm 3.8.10^3$ cells.cm^{-3}) was higher than the control, and the N and NSi enrichments, with mean values of respectively, $1.8.10^4$, $8.6.10^3 \pm 2.8.10^3$ and $7.3.10^3 \pm 2.3.10^3$ cells.cm^{-3}. NPSi enrichment showed the highest concentration of picoeukaryotes (mean = $5.4.10^4 \pm 1.5.10^4$ cells.cm^{-3}) (Kruskall-Wallis: $\chi^2 = 19.0$, $p_{value} = 7.9.10^{-4}$) (Fig. 7 C). Nanoeukaryotes also showed the highest concentration for NPSi enrichment with $9.9.10^4 \pm 3.4.10^4$ cells.cm^{-3} (Kruskall-Wallis: $\chi^2 = 13.3$, $p_{value} = 1.2.10^{-2}$, Conover: mean $p_{value} = 1.7.10^{-3}$). Regarding other treatments, controls contained higher concentrations of nanoeukaryotes ($2.4.10^3 \pm 8.8.10^2$ cells.cm^{-3}) than other enrichments with respectively $2.1.10^3 \pm 4.5.10^2$,$1.8.10^3 \pm 1.0.10^3$ and $1.9.10^3 \pm 9.1.10^2$ cells.cm^{-3} with P, N and NSi enrichments (Fig. 7 D). Cryptophytes exhibited the same trend as nanoeukaryotes with a higher concentration in the control than in P, N and NSi enrichments (Fig. 7 E) while NPSi

enrichment showed the significant higher concentration (χ^2 = 17.5, p_{value} = 1.4.10^{-3}, Conover: mean p_{value}= 4.2.10^{-3}), but the value may be too low to draw conclusion. Finally, with an initial concentration of 389 ± 166 cells.cm^{-3} *L. chlorophorum* decreased in all clusters except for the NPSi enrichment. The lowest concentration of 127 ± 26 cells.cm^{-3} was measured in controls while the highest was observed in NPSi enrichment with 1,876 ± 1,496 cells.cm^{-3}. The difference in NPSi enrichment observed in this species was highly significant (Kruskall-wallis: χ^2 = 18.5, p_{value} = 9.7.10^{-4}, Conover: mean = 2.2.10^{-4}) compared to in all the other enrichments (Fig. 7 F). The values measured for *L. chlorophorum* in the incubation are consistent with the maximum concentration value observed in august 2010, in the Bay of Seine by the French Observation and Monitoring program for Phytoplankton and Hydrology in coastal waters (REPHY , DOI: 10.17882/47248) with 418.3 cells.cm^{-3}.

Low values of APA 1.2.10^{-3} ± 1.5.10^{-4} nM.h^{-1}.mg chla^{-1}.l^{-1} were measured at D0 just after sampling. After incubation, APA increased in all enrichments by a factor of 15, 19; 24.8; 44.6; 4.4 respectively, in the control, P, N, NSi and NPSi enrichments compared to at D0. The minimum value of 6.6.10^{-3} ± 3.9.10^{-3} nM.h^{-1}.mg chla^{-1}.l^{-1} was observed in the NPSi cluster (Fig. 7 G) but no significant differences were found among enrichments (Kruskall-Wallis test). As observed for APA, the concentration of TEPincreased in all treatments except in the NPSi enrichment where TEP decreased. The concentration of TEP increased by a factor of 3 in the P enrichments (0.3 ± 0.05 µg Xanthan equ.µg chla^{-1}), by a factor 1.9 in both the N and NSi enrichments (0.5 ± 0.21 µg Xanthan equ.µg chla^{-1}). NPSi enrichment presented the lowest concentration (0.043 ± 0.03 µg Xanthan equ.µg chla^{-1}) but no significant differences were found among the treatments because of the high variability of the results between replications (Fig. 7 H).

Fv/Fm had a significantly high value in the NPSi enrichment with a mean of 0.46 ± 0.03 (Kruskall-Wallis: χ^2 = 10.6, p_{value} = 3.0.10^{-2}, Conover: mean p_{value}= 1.2.10^{-2}) (Fig 8. A) which is higher than the D0 value (0.41). The highest maximum production capacity ($JV_{II}max$) was also measured in the NPSi enrichments (Fig 8. B) with a value of 162 ± 77 mmol e$^-$.m^{-3}.h^{-1} revealing a

significant difference from that in the other treatments (Kruskall-Wallis : $\chi^2 = 9.7$, $p_{value} = 4.0.10^{-2}$, Conover: mean $p_{value} = 3.6.10^{-2}$) and again higher than the D0 value (6.1 mmol $e^-.m^{-3}.h^{-1}$). The highest electron transport rate ($ETR_{II}max$) was measured in the P and NSi enrichments (Fig 8. B) with values of respectively, 15.5 ± 5.2, 15.3 ± 6.5 mmol e^-.mg $chla^{-1}.h^{-1}$. A value of 8.1 ± 3.1 mmol e^-.mg $chla^{-1}.h^{-1}$ was measured in the NPSi enrichment but no significant differences were found between this and the other treatments (Kruskall-Wallis : $\chi^2 = 10.6$, $p_{value} = 3.0.10^{-2}$), Conover: mean pvalue = $7.6.10^{-2}$) (Fig 8. C), the value is however lower than the D0 value (21.7 mmol e^-.mg $chla^{-1}.h^{-1}$).

4. Discussion

The high frequency data provided by the instrumented buoy SMILE alerted us to the occurrence of a HAB bloom dominated by the Dinophyceae *Lepidodinium chlorophorum* in late August 2019, in the Bay of Seine. *L. chlorophorum* contained green chloroplasts probably derived from a prasinophyte endosymbiont (Hansen et al., 2007). Dinophyceae species with green chloroplasts are rare (Hansen et al., 2007) and to our knowledge *L. chlorophorum* is the only "green Dinophyceae" that has been identified in the English Channel (Sournia et al., 1992 and REPHY data base), so we were able to define a specific cytometric signature to characterise this species in our samples. The cytometric signature was confirmed in a strain isolated during the bloom thus allowing us to be extremely confident in our determination and the counting of *L. chlorophorum* in the present study. Although *L. chlorophorum* was first described in the English Channel in 1982 (Sournia et al., 1992), its ecology is still poorly documented. It is described as an euryhaline species, able to produce dinocysts (Elbrächter and Schnepf, 1996; Honsell and Talarico, 2004), with an optimum growth temperature of 22 °C established by Claquin et al. (2008) using a *L. chlorophorum* strain isolated in the English Channel. The conditions at the end of August 2019 were suitable to trigger a major *L. chlorophorum* bloom. The monitoring data from the SMILE buoy revealed the influence of nearby river outflows which, in summer, in the Bay of Seine, are defined

as warmer and more turbid freshwater inputs enriched in nutrients (Morelle et al., 2018; Napoléon et al., 2012). As already reported in many studies, these factors favour Dinophyceae blooms (Glibert, 2016), whose *L. chlorophorum* (Pozdnyakov et al., 2017) underlined the importance of rises in temperature while (Karasiewicz et al., 2020; Siano et al., 2018) pointed to the role of a drop in salinity during *L. chlorophorum* bloom events. Beside this general behaviour, which is widely described in the literature, our high-frequency data allowed us to monitor both the bloom and nutrient dynamics and the physiological state of the community in detail. The combination of a rise in temperature, a drop in salinity and nutrient inputs characteristic of estuarine waters triggered a bloom event in the bay which lasted six days on the monitoring site. After six days, the level of fluorescence dropped to its original value, marking the end of the bloom. The end of a bloom event can be triggered by different processes, such as a predatory (Tiselius and Kuylenstierna, 1996), virus event (Schroeder et al., 2003) or nutrient depletion (Walve and Larsson, 2007). In the present study, the high N/P ratio points to phosphate depletion. Thus, P appears to be a limiting nutrient and can be assumed to be the main driver of the decline in the bloom. Previous studies demonstrated that a bloom collapse can be explained by phosphate limitation (Walve and Larsson, 2007). The hypothesis of a P-limited bloom is supported in this study by the Fv/Fm value, which underwent a dramatic drop associated with a decline in biomass estimated by FFU one day after this drop. A value of 0.56 was measured for the Fv/Fm during the first three days of the bloom event, then decreased to 0.29 at mid bloom. This decrease could be partly due to a non-photochemical quenching mechanism (Harrison and Smith, 2013) but in our case, the minimum value appeared to be tightly linked to the increase in the N:P ratio. In the literature, a drop in the maximum quantum yield has been associated with nutrient limitation (Behrenfeld et al., 2004; Claquin et al., 2010), rapidly rising temperatures (Zhang et al., 2012), a change in salinity (D'ors et al., 2016), or even a parasitic event (Park et al., 2002). As *L. chlorophorum* tolerate a rise in sea temperature and a drop in salinity (Pozdnyakov et al., 2017; Siano et al., 2018), in our case, we assume that the decline in the maximum quantum yield was most likely caused by the phosphate limitation. P limitation has

been shown to significantly reduce the Fv/Fm in natural communities, in the field (Napoléon et al., 2012), in bioassays (Ly et al., 2014), and in lab cultures (Napoléon et al., 2013; Tan et al., 2019; Wongsnansilp et al., 2016; Wu et al., 2012). Besides, the maximum quantum yield decreased at mid bloom; the JV_{IImax} remained high because of the high level of biomass, and then dropped dramatically with the collapse of the bloom.

High-frequency sampling enabled by the SMILE buoy provided evidence for a link between P limitation and the collapse of a HAB bloom of *L. chlorophorum.* In a more general context, dinoflagellates have been associated with eutrophication since industrial development (Kim et al., 2018) and a recent shift has been observed (Fischer et al., 2020; Klais et al., 2013; Spilling et al., 2018) at global scale comprising an increase in the dinoflagellate/diatom ratio. Wasmund (2017) pointed to the relationship between an increase in the dinoflagellate/diatom ratio and a decrease in the quality indicator of environmental status assessment. The same trend has been described in the western English channel (Widdicombe et al., 2010) and in the Bay of Somme (Hernández-Fariñas et al., 2014). High-frequency monitoring allowed to understand and characterise short term processes and the factors which can trigger a large-scale bloom event and its fate. A bioassay enrichment experiment was performed during the bloom event to more deeply explore the behaviour and possible, control of bloom dynamics. Studying enrichments in a phytoplankton community involved in a natural bloom event is quite rare, and this enrichment bioassay enabled us to test other outcomes and their effects on phytoplankton communities as well as on several physiological indicators. However, the results obtained during the incubation have to be carefully consider in comparison with *in situ* data because the daily dynamics was not followed during the five days and many factors like hydrodynamics or grazing for example were removed. Beyond drawing a parallel between our microcosm experiments and our observations of a natural bloom, this second step of our study allowed us to investigate experimentally shifts in phytoplankton diversity during a HAB of *L. chlorophorum* and its effect on ecological functions such as primary productivity as a function of nutrient inputs. The relationship between primary productivity and biodiversity drives ecosystem

biomass production and is a therefore a major question of ecological functioning and ecosystem management (Hodapp et al., 2019).

The first outcome of this experiment was the remarkable behaviour of NPSi enrichment in comparison with other treatments. NPSi enrichment resulted in higher concentrations of almost all cytometric populations apart from *Synechococcus*. Bloom communities were not sustained by partial enrichment in N, or P or NSi. Only NPSi enrichment was able to trigger growth of the phytoplankton community. Unfortunately, an NP enrichment could not be performed because only five conditions could be tested into our incubator. Despite the absence of NP enrichment conditions, the experiment highlighted an apparent N, P co-limitation in this bioassay. N and P had to be added to significantly stimulate growth. Furthermore, it is important to note that in the NPSi enrichment, unlike Si, N and P were depleted. Such co-limitations have been extensively studied and discussed in coastal ecosystems (Davidson and Howarth, 2007) and NP inputs are known to promote dinoflagellate growth (Reynolds, 2006). During our experiments, the growth of all cytometric eukaryotic phytoplankton communities was stimulated under NPSi enrichment. Our results showed that the growth of *L .chlorophorum* was only stimulated in the fully replete condition.

A higher primary production capacity (JV_{IImax}) and a higher physiological status (Fv/Fm) were observed in the NPSi enrichment while lower productivity capacity (ETR_{IImax}) was measured in comparison with other treatments. The decoupling of production (JV_{IImax}) and productivity (ETR_{IImax}) in the NPSi enrichment was unexpected. This decoupling can be attributed to the size community structure, as differences in productivity between picoeucarykote, nanoeukaryote and microphytoplankton have been reported (Lefebvre et al., 2012; Li et al., 2011; Zhu et al., 2019) and may be one consequence of photoacclimatation processes. The increase in biomass in the NPSi enrichment reduced light penetration and increased self-shading (Huisman and Weissing, 1994) leading to an increase in the concentration of Chla in the photosystem antenna (Falkowski and LaRoche, 1991; MacIntyre et al., 2002). Such regulation has been associated with an internal increase in pigment self-shading, thereby reducing the pigment-specific light absorption coefficient

(σ_{PSII}) (Finkel et al., 2004). In our study, the lowest specific light absorption coefficient (σ_{PSII}) at 440 nm (Kolber et al., 1998) was measured in the NPSi enrichment (See supplementary data). Therefore, the self-shading mechanism makes it possible to explain the uncoupling observed between JV_{IImax} and ETR_{IImax} in these optimal growth conditions.

APA (as the potential maximum activity per chlorophyll unit) was quantified in order to characterise the P limitation during our experiment (Kuenzler and Perras, 1965; Lin et al., 2016; Tanaka et al., 2006). Alkaline phosphatase enables cells to access organic phosphate but the process is energy consuming (Falkowski and Raven, 1998; Lin et al., 2016). Dinoflagellates can make efficient use of dissolved organic phosphate (Wang et al., 2011), and quantifying APA is one way to asses this use when P is limited. According to the APA, the enrichment conditions applied in this bioassay can be gathered in three groups: (i) high P limitation for N and NSi, enrichments; (ii) medium P limitation for control and P and finally (iii) low P limitation for NPSi enrichment. The lack of any significant difference between controls and P enrichment despite the addition of P is surprising. P enrichment is N limited, which notably affects cell physiology. Previous studies showed that other limitations, like N (Kuenzler and Perras, 1965) or Si (Fuentes et al., 2014), can lead to an increase in APA. Changes in the community structure may also influence APA (Lin et al., 2015; Yuan et al., 2017). The observed differences in the picoeukaryote community under P replete conditions could alter nutrient uptake behaviour because picoeukaryotes are known to be very efficient in assimilating phosphorus. We hypothesise that this community produces more alkaline phosphatase than the other communities observed in the other enrichments. In addition, picoeukaryotes appeared to be favoured by P enrichment. This result showed that picoeukaryote was able to grow under N limitations, which are frequently reported in oligotrophic areas (MacKey et al., 2009; Siokou-Frangou et al., 2010) but rarely in eutrophic areas like the Bay of Seine where N limitation is only observed in summer (Napoléon et al., 2012; Thorel et al., 2017). Our results also showed that *Synechococcus* was unable to grow under any of the conditions we tested, which is

probably a bias introduced by our incubation methodology. The closed system could create greater predatory pressure leading to a higher death rate of *Synechococcus* (Agawin et al., 2000).

Si depletion did not occur either during the bloom event or during the bioassay, but even if Si was not limited during the course of this experiment, diatoms were not able to take over domination from dinoflagellates. In the literature, dinoflagellate dominance over diatoms is frequently reported to be driven by Si depletion (Liang et al., 2019; Zhou et al., 2017). Moreover, previous works showed that both in a natural bay (Lie et al., 2011) and in a model (Tett and Lee, 2005), when the N:Si ratio increases, the dinoflagellate/diatom ratio also increases. This supports our field measurements, which showed that environmental status (temperature and salinity) combined with an input of N and P triggered the dinoflagellate bloom even though Si was not limiting. Inputs of unbalanced nutrient water would not have triggered the bloom, as shown by the absence of growth in the experiment when only P or N were added.

TEP is widely associated with carbon excretion by phytoplankton (Claquin et al., 2008; Klein et al., 2011) even if bacteria can also promote TEP precursors (Li et al., 2016, 2015). Moreover, in the literature, TEP production is associated with N limitation (Beauvais et al., 2003; Corzo et al., 2000; Deng et al., 2016) or high N/P ratio (Mari et al., 2005). In our study, P, N, NSi enrichments displayed higher TEP concentrations per Chla unit. As mentioned previously, in all these experimental conditions, phytoplankton growth was limited in P or in N. Conversely, under non-limited growth conditions, i.e., the NPSi treatment, TEP production was reduced, which is physiologically coherent. Indeed, TEP can be considered as an overflow of carbon. As nutrient stresses do not allow proper carbon assimilation in the different metabolic pathways, carbon is accumulated as carbohydrates and part is excreted as TEP precursors. *L. chlorophorum* is described in the literature as a high TEP producer (Claquin et al., 2008; Sournia et al., 1992). Claquin et al., (2008) showed under replete conditions that *L. chlorophorum* was able to produce 10 times more TEP than other seven species tested which belonged to the main phytoplankton phyla. Such high TEP production favours the formation of aggregates and the sinking rate (Thornton, 2002) which

1 can lead to anoxia events that affect the benthos community (Passow, 2002). In the present study, an
2 O_2 depletion was observed at the end of the bloom; but although rare, this event was far from
3 anoxia.

4

5. Conclusions

In this study, the entire temporal pattern of a HAB species, *L. chlorophorum,* identified by microscopy and flow cytometry, was monitored. We showed that the high-frequency measurements of physical-chemical and biological parameters provided by the SMILE buoy allowed to detect the triggers of the bloom and its fate. There were not flow cytometer on the buoy, but our study pointed out that such a measurement associated with the others parameter available at high frequency would represent a great opportunity to deeper explorer phytoplankton dynamics and manage HAB events. The bioassay experiments performed during this bloom event allowed to explore physiological regulation at a community scale. The regulation of photosynthetic parameters was investigated as a function of nutrient inputs and of community structure, which made it possible to characterise uncoupling of production and productivity in some circumstances. The bioassay experiments also provided evidence of potential P and N co-limitation in this ecosystem and revealed that unbalanced inputs favour high TEP production with a population dominated by *L.chlorophorum*, which, in turn, can lead to massive bloom, sedimentation, and local oxygen depletion. Management of the nutrient inputs ratio has to be considered both in connection with the triggering - but also with the fate of blooms.

Acknowledgements

We thank Bertrand Le Roy from BOREA for *L. chlorophorum* isolation, Tania Hernández-Fariñas from Ifremer for her comments and advices and the COAST-HF network for technical support. This work was funded by the SMILE^2 and RIN ECUME projects respectively supported by *l'Agence de l'Eau Seine Normandie,*the European Regional Development Fund of Normandie, and *La Région Normandie* and by the PLEASE PhD project supported by *l'Agence de l'Eau Seine Normandie* and *La Région Normandie*

Agawin, N.S.R., Duarte, C.M., Agustí, S., 2000. Nutrient and temperature control of the contribution of picoplankton to phytoplankton biomass and production. Limnol. Oceanogr. 45, 591–600. https://doi.org/10.4319/lo.2000.45.3.0591

Aminot, A., Guillaud, J.-F., Andrieux-Loyer, F., Kérouel, R., Cann, P., 1998. Nutrients and phytoplanktonic growth in the Bay of Seine, France. Oceanol. Acta 6, 923–935.

Aminot, A., Kérouel, R., 2007. Dosage automatique des nutriments dans les eaux marines: méthodes en flux continu. Editions Quae.

Anderson, D.M., 2009. Approaches to monitoring, control and management of harmful algal blooms (HABs). Ocean Coast. Manag., Safer Coasts, Living with Risks: Selected Papers from the East Asian Seas Congress 2006, Haikou, Hainan, China 52, 342–347. https://doi.org/10.1016/j.ocecoaman.2009.04.006

Anderson, D.M., Glibert, P.M., Burkholder, J.M., 2002. Harmful algal blooms and eutrophication: Nutrient sources, composition, and consequences. Estuaries 25, 704–726. https://doi.org/10.1007/BF02804901

Azzaro, F., 2014. Automated Nutrients Analysis for Buoys in Sea-Water and Intercalibration. Int. J. Environ. Monit. Anal. 1, 315. https://doi.org/10.11648/j.ijema.20130106.17

Barbier, E.B., Hacker, S.D., Kennedy, C., Koch, E.W., Stier, A.C., Silliman, B.R., 2011. The value of estuarine and coastal ecosystem services. Ecol. Monogr. 81, 169–193. https://doi.org/10.1890/10-1510.1

Beauvais, S., Pedrotti, M.L., Villa, E., Lemée, R., 2003. Transparent exopolymer particle (TEP) dynamics in relation to trophic and hydrological conditions in the NW Mediterranean Sea. Mar. Ecol. Prog. Ser. 262, 97–109. https://doi.org/10.3354/meps262097

Behrenfeld, M.J., Prasil, O., Babin, M., Bruyant, F., 2004. In Search of a Physiological Basis for Covariations in Light-Limited and Light-Saturated Photosynthesis1. J. Phycol. 40, 4–25. https://doi.org/10.1046/j.1529-8817.2004.03083.x

Boatman, T.G., Geider, R.J., Oxborough, K., 2019. Improving the Accuracy of Single Turnover Active Fluorometry (STAF) for the Estimation of Phytoplankton Primary Productivity (PhytoPP). Front. Mar. Sci. 6. https://doi.org/10.3389/fmars.2019.00319

Bouman, H., Platt, T., Sathyendranath, S., Stuart, V., 2005. Dependence of light-saturated photosynthesis on temperature and community structure. Deep Sea Res. Part Oceanogr. Res. Pap. 52, 1284–1299. https://doi.org/10.1016/j.dsr.2005.01.008

Claquin, P., NÍ Longphuirt, S., Fouillaron, P., Huonnic, P., Ragueneau, O., Klein, C., Leynaert, A., 2010. Effects of simulated benthic fluxes on phytoplankton dynamic and photosynthetic parameters in a mesocosm experiment (Bay of Brest, France). Estuar. Coast. Shelf Sci. 86, 93–101. https://doi.org/10.1016/j.ecss.2009.10.017

Claquin, P., Probert, I., Lefebvre, S., Veron, B., 2008. Effects of temperature on photosynthetic parameters and TEP production in eight species of marine microalgae. Aquat. Microb. Ecol. 51, 1–11. https://doi.org/10.3354/ame01187

Corzo, A., Morillo, J.A., Rodríguez, S., 2000. Production of transparent exopolymer particles (TEP) in cultures of *Chaetoceros calcitrans* under nitrogen limitation. Aquat. Microb. Ecol. 23, 63–72. https://doi.org/10.3354/ame023063

Davidson, E.A., Howarth, R.W., 2007. Nutrients in synergy. Nature 449, 1000–1001. https://doi.org/10.1038/4491000a

Deng, W., Cruz, B.N., Neuer, S., 2016. Effects of nutrient limitation on cell growth, TEP production and aggregate formation of marine *Synechococcus*. Aquat. Microb. Ecol. 78, 39–49. https://doi.org/10.3354/ame01803

D'ors, A., Bartolomé, M.C., Sánchez-Fortún, S., 2016. Repercussions of salinity changes and osmotic stress in marine phytoplankton species. Estuar. Coast. Shelf Sci. 175, 169–175. https://doi.org/10.1016/j.ecss.2016.04.004

Elbrächter, M., Schnepf, E., 1996. *Gymnodinium chlorophorum*, a new, green, bloom-forming dinoflagellate (Gymnodiniales, Dinophyceae) with a vestigial prasinophyte endosymbiont. Phycologia 35, 381–393. https://doi.org/10.2216/i0031-8884-35-5-381.1

Falkowski, P.G., LaRoche, J., 1991. Acclimation to Spectral Irradiance in Algae. J. Phycol. 27, 8–14. https://doi.org/10.1111/j.0022-3646.1991.00008.x

Falkowski, P.G., Raven, J.A., 1998. Review of Aquatic Photosynthesis. New Phytol. 140, 597–598.

Finkel, Z.V., Irwin, A.J., Schofield, O., 2004. Resource limitation alters the 3/4 size scaling of metabolic rates in phytoplankton. Mar. Ecol. Prog. Ser. 273, 269–279. https://doi.org/10.3354/meps273269

Fischer, A.D., Hayashi, K., McGaraghan, A., Kudela, R.M., 2020. Return of the "age of dinoflagellates" in Monterey Bay: Drivers of dinoflagellate dominance examined using automated imaging flow cytometry and long-term time series analysis. Limnol. Oceanogr. 65, 2125–2141. https://doi.org/10.1002/lno.11443

Fuentes, S., Wikfors, G.H., Meseck, S., 2014. Silicon Deficiency Induces Alkaline Phosphatase Enzyme Activity in Cultures of Four Marine Diatoms. Estuaries Coasts 37, 312–324. https://doi.org/10.1007/s12237-013-9695-z

Garnier, J., Riou, P., Le Gendre, R., Ramarson, A., Billen, G., Cugier, P., Schapira, M., Théry, S., Thieu, V., Ménesguen, A., 2019. Managing the Agri-Food System of Watersheds to Combat Coastal Eutrophication: A Land-to-Sea Modelling Approach to the French Coastal English Channel. Geosciences 9, 441. https://doi.org/10.3390/geosciences9100441

Genty, B., Briantais, J.-M., Baker, N.R., 1989. The relationship between the quantum yield of photosynthetic electron transport and quenching of chlorophyll fluorescence. Biochim. Biophys. Acta BBA - Gen. Subj. 990, 87–92. https://doi.org/10.1016/S0304-4165(89)80016-9

Glibert, P.M., 2016. Margalef revisited: A new phytoplankton mandala incorporating twelve dimensions, including nutritional physiology. Harmful Algae 55, 25–30. https://doi.org/10.1016/j.hal.2016.01.008

Gohin, F., Van der Zande, D., Tilstone, G., Eleveld, M.A., Lefebvre, A., Andrieux-Loyer, F., Blauw, A.N., Bryère, P., Devreker, D., Garnesson, P., Hernández Fariñas, T., Lamaury, Y., Lampert, L., Lavigne, H., Menet-Nedelec, F., Pardo, S., Saulquin, B., 2019. Twenty years of satellite and in situ observations of surface chlorophyll-a from the northern Bay of Biscay to the eastern English Channel. Is the water quality improving? Remote Sens. Environ. 233, 111343. https://doi.org/10.1016/j.rse.2019.111343

Granéli, E., Weberg, M., Salomon, P.S., 2008. Harmful algal blooms of allelopathic microalgal species: The role of eutrophication. Harmful Algae, HABs and Eutrophication 8, 94–102. https://doi.org/10.1016/j.hal.2008.08.011

Hansen, G., Botes, L., Salas, M.D., 2007. Ultrastructure and large subunit rDNA sequences of *Lepidodinium viride* reveal a close relationship to *Lepidodinium chlorophorum* comb. nov. (=*Gymnodinium chlorophorum*). Phycol. Res. 55, 25–41. https://doi.org/10.1111/j.1440-1835.2006.00442.x

Harrison, J.W., Smith, R.E.H., 2013. Effects of nutrients and irradiance on PSII variable fluorescence of lake phytoplankton assemblages. Aquat. Sci. 75, 399–411. https://doi.org/10.1007/s00027-012-0285-0

Heisler, J., Glibert, P.M., Burkholder, J.M., Anderson, D.M., Cochlan, W., Dennison, W.C., Dortch, Q., Gobler, C.J., Heil, C.A., Humphries, E., Lewitus, A., Magnien, R., Marshall, H.G., Sellner, K., Stockwell, D.A., Stoecker, D.K., Suddleson, M., 2008. Eutrophication and harmful algal blooms: A scientific consensus. Harmful Algae, HABs and Eutrophication 8, 3–13. https://doi.org/10.1016/j.hal.2008.08.006

Hernández-Fariñas, T., Soudant, D., Barillé, L., Belin, C., Lefebvre, A., Bacher, C., 2014. Temporal changes in the phytoplankton community along the French coast of the eastern English

Channel and the southern Bight of the North Sea. ICES J. Mar. Sci. 71, 821–833. https://doi.org/10.1093/icesjms/fst192

Hodapp, D., Hillebrand, H., Striebel, M., 2019. “Unifying” the Concept of Resource Use Efficiency in Ecology. Front. Ecol. Evol. 6. https://doi.org/10.3389/fevo.2018.00233

Honsell, G., Talarico, L., 2004. *Gymnodinium chlorophorum* (Dinophyceae) in the Adriatic Sea: electron microscopical observations. Bot. Mar. 47, 152–166. https://doi.org/10.1515/BOT.2004.016

Hrustic, E., Lignell, R., Riebesell, U., Thingstad, T.F., 2017. Exploring the distance between nitrogen and phosphorus limitation in mesotrophic surface waters using a sensitive bioassay. Biogeosciences 14, 379–387. https://doi.org/10.5194/bg-14-379-2017

Huisman, J., Weissing, F.J., 1994. Light-Limited Growth and Competition for Light in Well-Mixed Aquatic Environments: An Elementary Model. Ecology 75, 507–520. https://doi.org/10.2307/1939554

Karasiewicz, S., Chapelle, A., Bacher, C., Soudant, D., 2020. Harmful algae niche responses to environmental and community variation along the French coast. Harmful Algae 93, 101785. https://doi.org/10.1016/j.hal.2020.101785

Kim, S.-Y., Roh, Y.H., Shin, H.H., Huh, S., Kang, S.-H., Lim, D., 2018. Decadal-scale variations of sedimentary dinoflagellate cyst records from the Yellow Sea over the last 400 years. Estuar. Coast. Shelf Sci. 200, 91–98. https://doi.org/10.1016/j.ecss.2017.10.006

Klais, R., Tamminen, T., Kremp, A., Spilling, K., An, B.W., Hajdu, S., Olli, K., 2013. Spring phytoplankton communities shaped by interannual weather variability and dispersal limitation: Mechanisms of climate change effects on key coastal primary producers. Limnol. Oceanogr. 58, 753–762. https://doi.org/10.4319/lo.2013.58.2.0753

Klein, C., Claquin, P., Pannard, A., Napoléon, C., Roy, B.L., Véron, B., 2011. Dynamics of soluble extracellular polymeric -substances and transparent exopolymer particle pools in coastal ecosystems. Mar. Ecol. Prog. Ser. 427, 13–27. https://doi.org/10.3354/meps09049

Kolber, Z.S., Prášil, O., Falkowski, P.G., 1998. Measurements of variable chlorophyll fluorescence using fast repetition rate techniques: defining methodology and experimental protocols. Biochim. Biophys. Acta BBA - Bioenerg. 1367, 88–106. https://doi.org/10.1016/S0005-2728(98)00135-2

Kuenzler, E.J., Perras, J.P., 1965. Phosphatases of marine algae. Biol. Bull. 128, 271–284. https://doi.org/10.2307/1539555

Lefebvre, S., Claquin, P., Orvain, F., Véron, B., Charpy, L., 2012. Spatial and temporal dynamics of size-structured photosynthetic parameters (PAM) and primary production (13C) of pico- and nano-phytoplankton in an atoll lagoon. Mar. Pollut. Bull., Ahe Atoll and Pearl Oyster Aquaculture in the Tuamotu Archipelago 65, 478–489. https://doi.org/10.1016/j.marpolbul.2012.04.011

Lefort, T., Gasol, J.M., 2014. Short-time scale coupling of picoplankton community structure and single-cell heterotrophic activity in winter in coastal NW Mediterranean Sea waters. J. Plankton Res. 36, 243–258. https://doi.org/10.1093/plankt/fbt073

Lemesle, S., Mussio, I., Rusig, A.-M., Menet-Nédélec, F., Claquin, P., 2015. Impact of seaweed beachings on dynamics of δ15N isotopic signatures in marine macroalgae. Mar. Pollut. Bull. 97, 241–254. https://doi.org/10.1016/j.marpolbul.2015.06.010

Leruste, A., Pasqualini, V., Garrido, M., Malet, N., De Wit, R., Bec, B., 2019. Physiological and behavioral responses of phytoplankton communities to nutrient availability in a disturbed Mediterranean coastal lagoon. Estuar. Coast. Shelf Sci. 219, 176–188. https://doi.org/10.1016/j.ecss.2019.02.014

Li, B., Karl, D.M., Letelier, R.M., Church, M.J., 2011. Size-dependent photosynthetic variability in the North Pacific Subtropical Gyre. Mar. Ecol. Prog. Ser. 440, 27–40. https://doi.org/10.3354/meps09345

Li, S., Winters, H., Jeong, S., Emwas, A.-H., Vigneswaran, S., Amy, G.L., 2016. Marine bacterial transparent exopolymer particles (TEP) and TEP precursors: Characterization and RO fouling potential. Desalination 379, 68–74. https://doi.org/10.1016/j.desal.2015.10.005

Li, S., Winters, H., Villacorte, L.O., Ekowati, Y., Emwas, A.-H., Kennedy, M.D., Amy, G.L., 2015. Compositional similarities and differences between transparent exopolymer particles (TEPs) from two marine bacteria and two marine algae: Significance to surface biofouling. Mar. Chem. 174, 131–140. https://doi.org/10.1016/j.marchem.2015.06.009

Liang, Y., Zhang, G., Wan, A., Zhao, Z., Wang, S., Liu, Q., 2019. Nutrient-limitation induced diatom-dinoflagellate shift of spring phytoplankton community in an offshore shellfish farming area. Mar. Pollut. Bull. 141, 1–8. https://doi.org/10.1016/j.marpolbul.2019.02.009

Lie, A.A.Y., Wong, C.K., Lam, J.Y.C., Liu, J.H., Yung, Y.K., 2011. Changes in the nutrient ratios and phytoplankton community after declines in nutrient concentrations in a semi-enclosed bay in Hong Kong. Mar. Environ. Res. 71, 178–188. https://doi.org/10.1016/j.marenvres.2011.01.001

Lin, S., Litaker, R.W., Sunda, W.G., 2016. Phosphorus physiological ecology and molecular mechanisms in marine phytoplankton. J. Phycol. 52, 10–36. https://doi.org/10.1111/jpy.12365

Lin, X., Wang, L., Shi, X., Lin, S., 2015. Rapidly diverging evolution of an atypical alkaline phosphatase (PhoAaty) in marine phytoplankton: insights from dinoflagellate alkaline phosphatases. Front. Microbiol. 6. https://doi.org/10.3389/fmicb.2015.00868

Ly, J., Philippart, C.J.M., Kromkamp, J.C., 2014. Phosphorus limitation during a phytoplankton spring bloom in the western Dutch Wadden Sea. J. Sea Res. 88, 109–120. https://doi.org/10.1016/j.seares.2013.12.010

MacIntyre, H.L., Kana, T.M., Anning, T., Geider, R.J., 2002. Photoacclimation of Photosynthesis Irradiance Response Curves and Photosynthetic Pigments in Microalgae and Cyanobacteria1. J. Phycol. 38, 17–38. https://doi.org/10.1046/j.1529-8817.2002.00094.x

MacKey, K.R.M., Rivlin, T., Grossman, A.R., Post, A.F., Paytan, A., 2009. Picophytoplankton responses to changing nutrient and light regimes during a bloom. Mar. Biol. 156, 1531–1546. https://doi.org/10.1007/s00227-009-1185-2

Mari, X., Rassoulzadegan, F., Brussaard, C.P.D., Wassmann, P., 2005. Dynamics of transparent exopolymeric particles (TEP) production by *Phaeocystis globosa* under N- or P-limitation: a controlling factor of the retention/export balance. Harmful Algae, Bloom Dynamics and Biological Control of *Phaeocystis*: a HAB Species in European Coastal Waters 4, 895–914. https://doi.org/10.1016/j.hal.2004.12.014

Martin, G.D., Vijay, J.G., Laluraj, C.M., Madhu, N.V., Joseph, T., Nair, M., Gupta, G.V.M., Balachandran, K.K., 2008. Fresh water influence on nutrient stoichiometry in a tropical estuary, Southwest coast of India. Appl. Ecol. Environ. Res.

Meybeck, M., Lestel, L., Carré, C., Bouleau, G., Garnier, J., Mouchel, J.M., 2018. Trajectories of river chemical quality issues over the Longue Durée: the Seine River (1900S–2010). Environ. Sci. Pollut. Res. 25, 23468–23484. https://doi.org/10.1007/s11356-016-7124-0

Morelle, J., Schapira, M., Orvain, F., Riou, P., Lopez, P.J., Pierre-Duplessix, O., Rabiller, E., Maheux, F., Simon, B., Claquin, P., 2018. Annual Phytoplankton Primary Production Estimation in a Temperate Estuary by Coupling PAM and Carbon Incorporation Methods. Estuaries Coasts 41, 1337–1355. https://doi.org/10.1007/s12237-018-0369-8

Moscetta, P., Sanfilippo, L., Savino, E., Moscetta, P., Allabashi, R., Gunatilaka, A., 2009. Instrumentation for continuous monitoring in marine environments, in: OCEANS 2009. Presented at the OCEANS 2009, pp. 1–10. https://doi.org/10.23919/OCEANS.2009.5422370

Napoléon, C., Fiant, L., Raimbault, V., Riou, P., Claquin, P., 2014. Dynamics of phytoplankton diversity structure and primary productivity in the English Channel. Mar. Ecol. Prog. Ser. 505, 49–64. https://doi.org/10.3354/meps10772

Napoléon, C., Raimbault, V., Claquin, P., 2013. Influence of Nutrient Stress on the Relationships between PAM Measurements and Carbon Incorporation in Four Phytoplankton Species. PLOS ONE 8, e66423. https://doi.org/10.1371/journal.pone.0066423

Napoléon, C., Raimbault, V., Fiant, L., Riou, P., Lefebvre, S., Lampert, L., Claquin, P., 2012. Spatiotemporal dynamics of physicochemical and photosynthetic parameters in the central English Channel. J. Sea Res. 69, 43–52. https://doi.org/10.1016/j.seares.2012.01.005

Nwankwegu, A.S., Li, Y., Huang, Y., Wei, J., Norgbey, E., Lai, Q., Sarpong, L., Wang, K., Ji, D., Yang, Z., Paerl, H.W., 2020. Nutrient addition bioassay and phytoplankton community structure monitored during autumn in Xiangxi Bay of Three Gorges Reservoir, China. Chemosphere 247, 125960. https://doi.org/10.1016/j.chemosphere.2020.125960

Olson, R.J., Zettler, E.R., Anderson, O.K., 1989. Discrimination of eukaryotic phytoplankton cell types from light scatter and autofluorescence properties measured by flow cytometry. Cytometry 10, 636–643. https://doi.org/10.1002/cyto.990100520

Oxborough, K., Moore, C.M., Suggett, D.J., Lawson, T., Chan, H.G., Geider, R.J., 2012. Direct estimation of functional PSII reaction center concentration and PSII electron flux on a volume basis: a new approach to the analysis of Fast Repetition Rate fluorometry (FRRf) data. Limnol. Oceanogr. Methods 10, 142–154. https://doi.org/10.4319/lom.2012.10.142

Park, M.G., Cooney, S.K., Yih, W., Coats, D.W., 2002. Effects of two strains of the parasitic dinoflagellate *Amoebophrya* on growth, photosynthesis, light absorption, and quantum yield of bloom-forming dinoflagellates. Mar. Ecol. Prog. Ser. 227, 281–292. https://doi.org/10.3354/meps227281

Passow, U., 2002. Transparent exopolymer particles (TEP) in aquatic environments. Prog. Oceanogr. 55, 287–333. https://doi.org/10.1016/S0079-6611(02)00138-6

Passow, U., Alldredge, A.L., 1996. A dye-binding assay for the spectrophotometric measurement of transparent exopolymer particles (TEP). Oceanogr. Lit. Rev. 7, 669.

Pozdnyakov, D.V., Pettersson, L.H., Korosov, A.A., 2017. Investigation of Harmful/Nuisance Algae Blooms in Marine Environments, in: Pozdnyakov, D.V., Pettersson, L.H., Korosov, A.A. (Eds.), Exploring the Marine Ecology from Space: Experience from Russian-Norwegian Cooperation, Springer Remote Sensing/Photogrammetry. Springer International Publishing, Cham, pp. 95–140. https://doi.org/10.1007/978-3-319-30075-7_3

Rabalais, N.N., Turner, R.E., Díaz, R.J., Justić, D., 2009. Global change and eutrophication of coastal waters. ICES J. Mar. Sci. 66, 1528–1537. https://doi.org/10.1093/icesjms/fsp047

Reynolds, C.S., 2006. The Ecology of Phytoplankton, Ecology, Biodiversity and Conservation. Cambridge University Press, Cambridge. https://doi.org/10.1017/CBO9780511542145

Schroeder, D.C., Oke, J., Hall, M., Malin, G., Wilson, W.H., 2003. Virus Succession Observed during an *Emiliania huxleyi* Bloom. Appl. Environ. Microbiol. 69, 2484–2490. https://doi.org/10.1128/AEM.69.5.2484-2490.2003

Shen, Z.-L., 2001. Historical Changes in Nutrient Structure and its Influences on Phytoplantkon Composition in Jiaozhou Bay. Estuar. Coast. Shelf Sci. 52, 211–224. https://doi.org/10.1006/ecss.2000.0736

Siano, R., Chapelle, A., Antoine, V., Michel-Guillou, E., Rigaut-Jalabert, F., Guillou, L., Hégaret, H., Leynaert, A., Curd, A., 2018. Citizen participation in monitoring phytoplankton seawater discolorations. Mar. Policy. https://doi.org/10.1016/j.marpol.2018.01.022

Siokou-Frangou, I., Christaki, U., Mazzocchi, M.G., Montresor, M., Ribera d'Alcalá, M., Vaqué, D., Zingone, A., 2010. Plankton in the open Mediterranean Sea: a review. Biogeosciences 7, 1543–1586. https://doi.org/10.5194/bg-7-1543-2010

Smith, V.H., 2006. Responses of estuarine and coastal marine phytoplankton to nitrogen and phosphorus enrichment. Limnol. Oceanogr. 51, 377–384. https://doi.org/10.4319/lo.2006.51.1_part_2.0377

Sournia, A., Belin, C., Billard, C., Catherine, M., Erard-Le Denn, E., Fresnel, J., Lassus, P., Pastoureaud, A., Soulard, R., 1992b. The repetitive and expanding occurrence of a green,

bloom-forming dinoflagellate (Dinophyceae) on the coasts of France. Cryptogam. Algol. 13, 1–13.

Spilling, K., Olli, K., Lehtoranta, J., Kremp, A., Tedesco, L., Tamelander, T., Klais, R., Peltonen, H., Tamminen, T., 2018. Shifting Diatom—Dinoflagellate Dominance During Spring Bloom in the Baltic Sea and its Potential Effects on Biogeochemical Cycling. Front. Mar. Sci. 5. https://doi.org/10.3389/fmars.2018.00327

Strickland, J.D.H., Parsons, T.R., 1972. A Practical Handbook of Seawater Analysis. Bull. Fish. Res. Board Can. 310.

Tan, L., Xu, W., He, X., Wang, J., 2019. The feasibility of Fv/Fm on judging nutrient limitation of marine algae through indoor simulation and in situ experiment. Estuar. Coast. Shelf Sci. 229, 106411. https://doi.org/10.1016/j.ecss.2019.106411

Tanaka, T., Henriksen, P., Lignell, R., Olli, K., Seppälä, J., Tamminen, T., Thingstad, T.F., 2006. Specific Affinity for Phosphate Uptake and Specific Alkaline Phosphatase Activity as Diagnostic Tools for Detecting Phosphorus-Limited Phytoplankton and Bacteria. Estuaries Coasts 29, 1226–1241.

Tett, P., Lee, J.-Y., 2005. N:Si ratios and the 'balance of organisms': PROWQM simulations of the northern North Sea. J. Sea Res., Contrasting Approaches to Understanding Eutrophication Effects on Phytoplankton 54, 70–91. https://doi.org/10.1016/j.seares.2005.02.012

Thorel, M., Claquin, P., Schapira, M., Le Gendre, R., Riou, P., Goux, D., Le Roy, B., Raimbault, V., Deton-Cabanillas, A.-F., Bazin, P., Kientz-Bouchart, V., Fauchot, J., 2017. Nutrient ratios influence variability in *Pseudo-nitzschia* species diversity and particulate domoic acid production in the Bay of Seine (France). Harmful Algae 68, 192–205. https://doi.org/10.1016/j.hal.2017.07.005

Thornton, D., 2002. Diatom aggregation in the sea: mechanisms and ecological implications. Eur. J. Phycol. 37, 149–161. https://doi.org/10.1017/S0967026202003657

Thyssen, M., Grégori, G.J., Grisoni, J.-M., Pedrotti, M.L., Mousseau, L., Artigas, L.F., Marro, S., Garcia, N., Passafiume, O., Denis, M.J., 2014. Onset of the spring bloom in the northwestern Mediterranean Sea: influence of environmental pulse events on the in situ hourly-scale dynamics of the phytoplankton community structure. Front. Microbiol. 5. https://doi.org/10.3389/fmicb.2014.00387

Thyssen, M., Tarran, G.A., Zubkov, M.V., Holland, R.J., Grégori, G., Burkill, P.H., Denis, M., 2008. The emergence of automated high-frequency flow cytometry: revealing temporal and spatial phytoplankton variability. J. Plankton Res. 30, 333–343. https://doi.org/10.1093/plankt/fbn005

Tiselius, P., Kuylenstierna, M., 1996. Growth and decline of a diatom spring bloom phytoplankton species composition, formation of marine snow and the role of heterotrophic dinoflagellates. J. Plankton Res. 18, 133–155. https://doi.org/10.1093/plankt/18.2.133

Walve, J., Larsson, U., 2007. Blooms of Baltic Sea *Aphanizomenon* sp. (Cyanobacteria) collapse after internal phosphorus depletion. Aquat. Microb. Ecol. 49, 57–69. https://doi.org/10.3354/ame01130

Wang, Z., Liang, Y., Kang, W., 2011. Utilization of dissolved organic phosphorus by different groups of phytoplankton taxa. Harmful Algae 12, 113–118. https://doi.org/10.1016/j.hal.2011.09.005

Wasmund, N., 2017. The Diatom/Dinoflagellate Index as an Indicator of Ecosystem Changes in the Baltic Sea. 2. Historical Data for Use in Determination of Good Environmental Status. Front. Mar. Sci. 4. https://doi.org/10.3389/fmars.2017.00153

Watanabe, K., Kasai, A., Fukuzaki, K., Ueno, M., Yamashita, Y., 2017. Estuarine circulation-driven entrainment of oceanic nutrients fuels coastal phytoplankton in an open coastal system in Japan. Estuar. Coast. Shelf Sci. 184, 126–137. https://doi.org/10.1016/j.ecss.2016.10.031

Webb, W.L., Newton, M., Starr, D., 1974. Carbon dioxide exchange of *Alnus rubra* : A mathematical model. Oecologia 17, 281–291. https://doi.org/10.1007/BF00345747

Widdicombe, C.E., Eloire, D., Harbour, D., Harris, R.P., Somerfield, P.J., 2010. Long-term phytoplankton community dynamics in the Western English Channel. J. Plankton Res. 32, 643–655. https://doi.org/10.1093/plankt/fbp127

Wongsnansilp, T., Juntawong, N., Wu, Z., 2016. Effects of phosphorus on the growth and chlorophyll fluorescence of a *Dunaliella salina* strain isolated from saline soil under nitrate limitation. J. Biol. Res.-Boll. Della Soc. Ital. Biol. Sper. 89, 51–55. https://doi.org/10.4081/jbr.2016.5866

Wu, Z., Zeng, B., Li, R., Song, L., 2012. Physiological regulation of *Cylindrospermopsis raciborskii* (Nostocales, Cyanobacteria) in response to inorganic phosphorus limitation. Harmful Algae 15, 53–58. https://doi.org/10.1016/j.hal.2011.11.005

Yuan, Y., Bi, Y., Hu, Z., 2017. Phytoplankton communities determine the spatio-temporal heterogeneity of alkaline phosphatase activity: evidence from a tributary of the Three Gorges Reservoir. Sci. Rep. 7, 16404. https://doi.org/10.1038/s41598-017-16740-4

Zhang, M., Yu, Y., Yang, Z., Kong, F., 2012. Photochemical responses of phytoplankton to rapid increasing-temperature process. Phycol. Res. 60, 199–207. https://doi.org/10.1111/j.1440-1835.2012.00654.x

Zhou, Y., Zhang, Y., Li, F., Tan, L., Wang, J., 2017. Nutrients structure changes impact the competition and succession between diatom and dinoflagellate in the East China Sea. Sci. Total Environ. 574, 499–508. https://doi.org/10.1016/j.scitotenv.2016.09.092

Zhu, Y., Suggett, D.J., Liu, C., He, J., Lin, L., Le, F., Ishizaka, J., Goes, J., Hao, Q., 2019. Primary Productivity Dynamics in the Summer Arctic Ocean Confirms Broad Regulation of the Electron Requirement for Carbon Fixation by Light-Phytoplankton Community Interaction. Front. Mar. Sci. 6. https://doi.org/10.3389/fmars.2019.00275

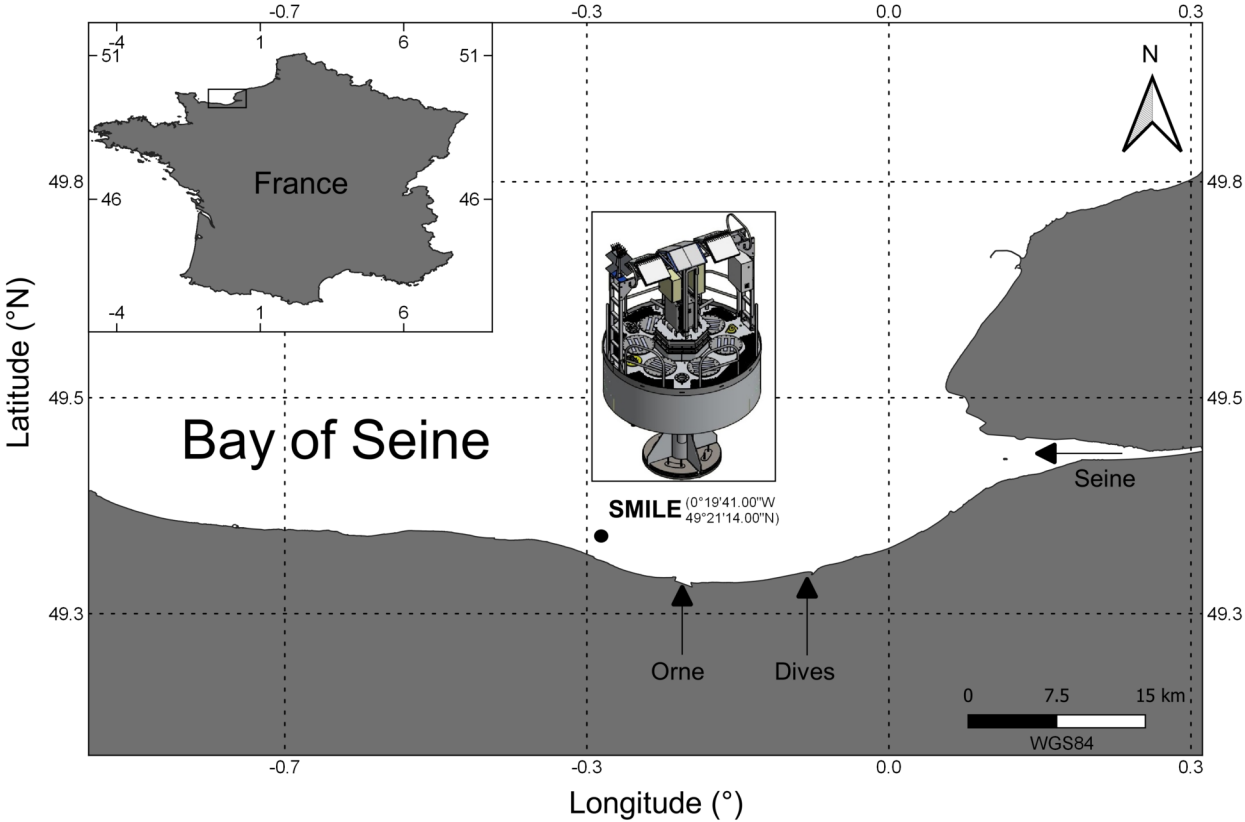
-0.7
-0.3
0.0
0.3
N
49.8
49.5
49.3
Latitude (°N)
Longitude (°)
-4
1
6
51
46
France
Bay of Seine
SMILE (0°19'41.00"W 49°21'14.00"N)
Seine
Orne
Dives
0
7.5
15 km
WGS84

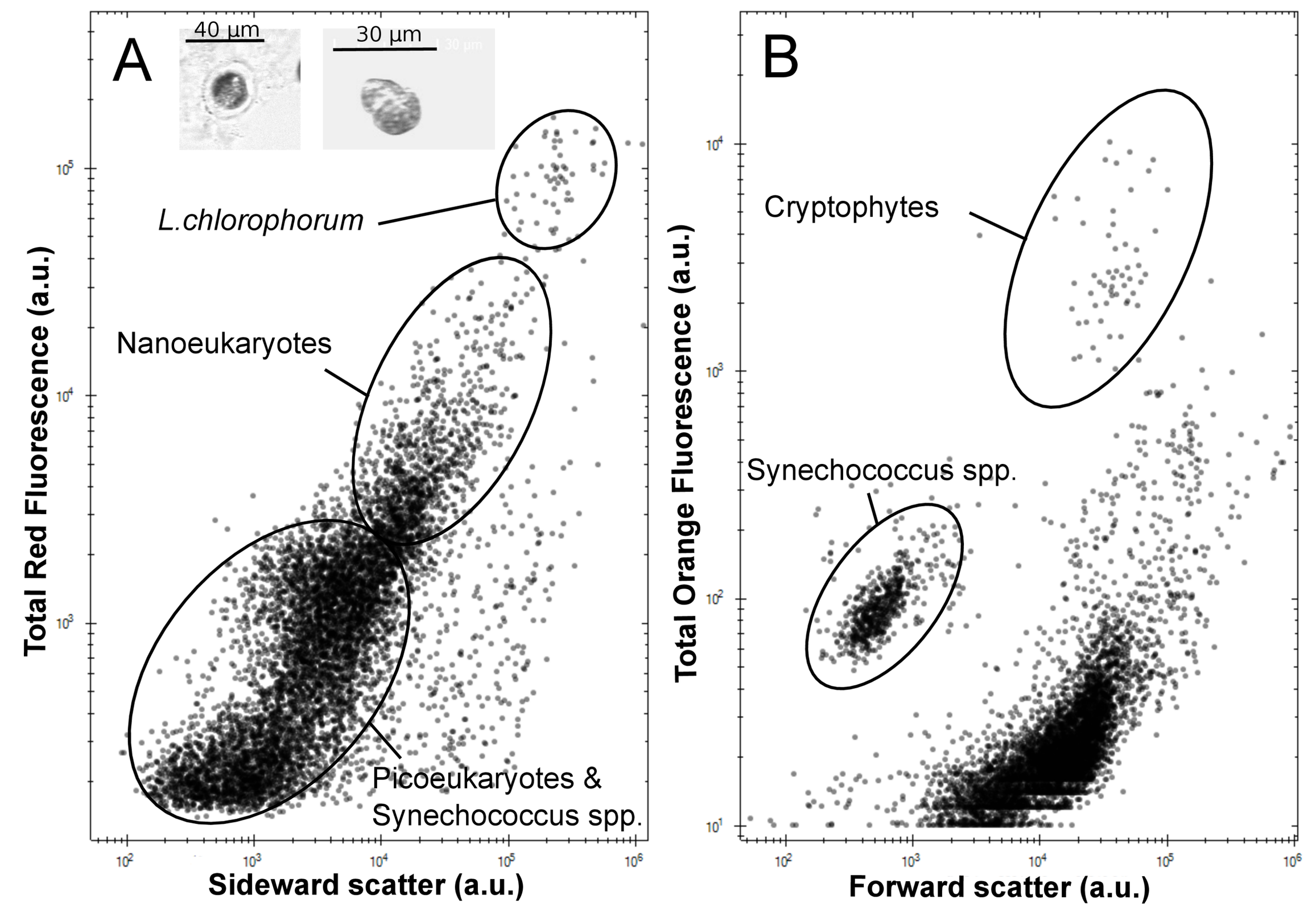
A
40 µm
30 µm
L.chlorophorum
Nanoeukaryotes
Picoeukaryotes &
Synechococcus spp.
Total Red Fluorescence (a.u.)
Sideward scatter (a.u.)
B
Cryptophytes
Synechococcus spp.
Total Orange Fluorescence (a.u.)
Forward scatter (a.u.)

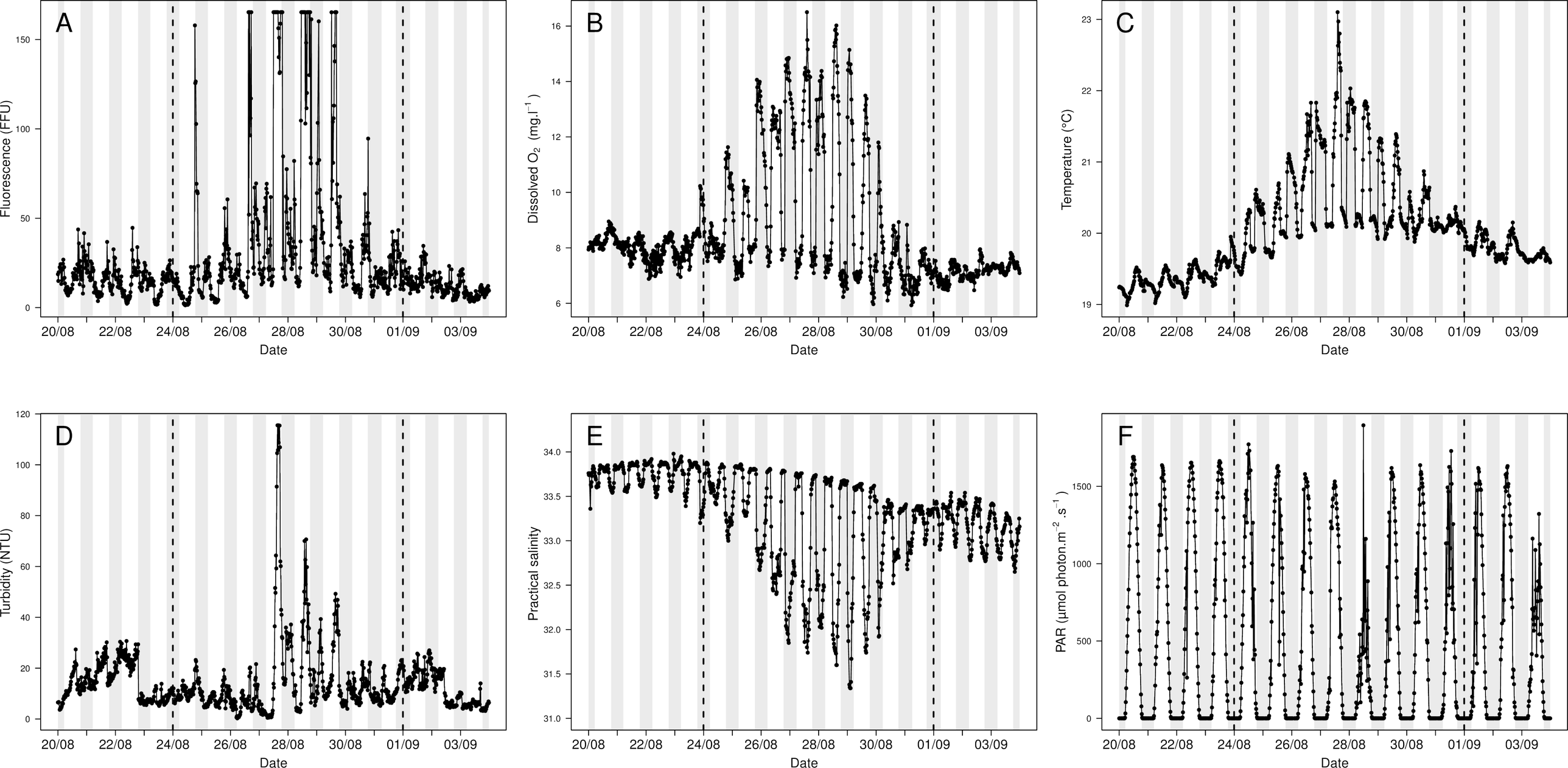
A
Fluorescence (FFU)
0
50
100
150
20/08
22/08
24/08
26/08
28/08
30/08
01/09
03/09
Date
B
Dissolved O_2 (mg.l^{-1})
6
8
10
12
14
16
20/08
22/08
24/08
26/08
28/08
30/08
01/09
03/09
Date
C
Temperature (°C)
19
20
21
22
23
20/08
22/08
24/08
26/08
28/08
30/08
01/09
03/09
Date
D
Turbidity (NTU)
0
20
40
60
80
100
120
20/08
22/08
24/08
26/08
28/08
30/08
01/09
03/09
Date
E
Practical salinity
31.0
31.5
32.0
32.5
33.0
33.5
34.0
20/08
22/08
24/08
26/08
28/08
30/08
01/09
03/09
Date
F
PAR (µmol photon.m^{-2}.s^{-1})
0
500
1000
1500
20/08
22/08
24/08
26/08
28/08
30/08
01/09
03/09
Date

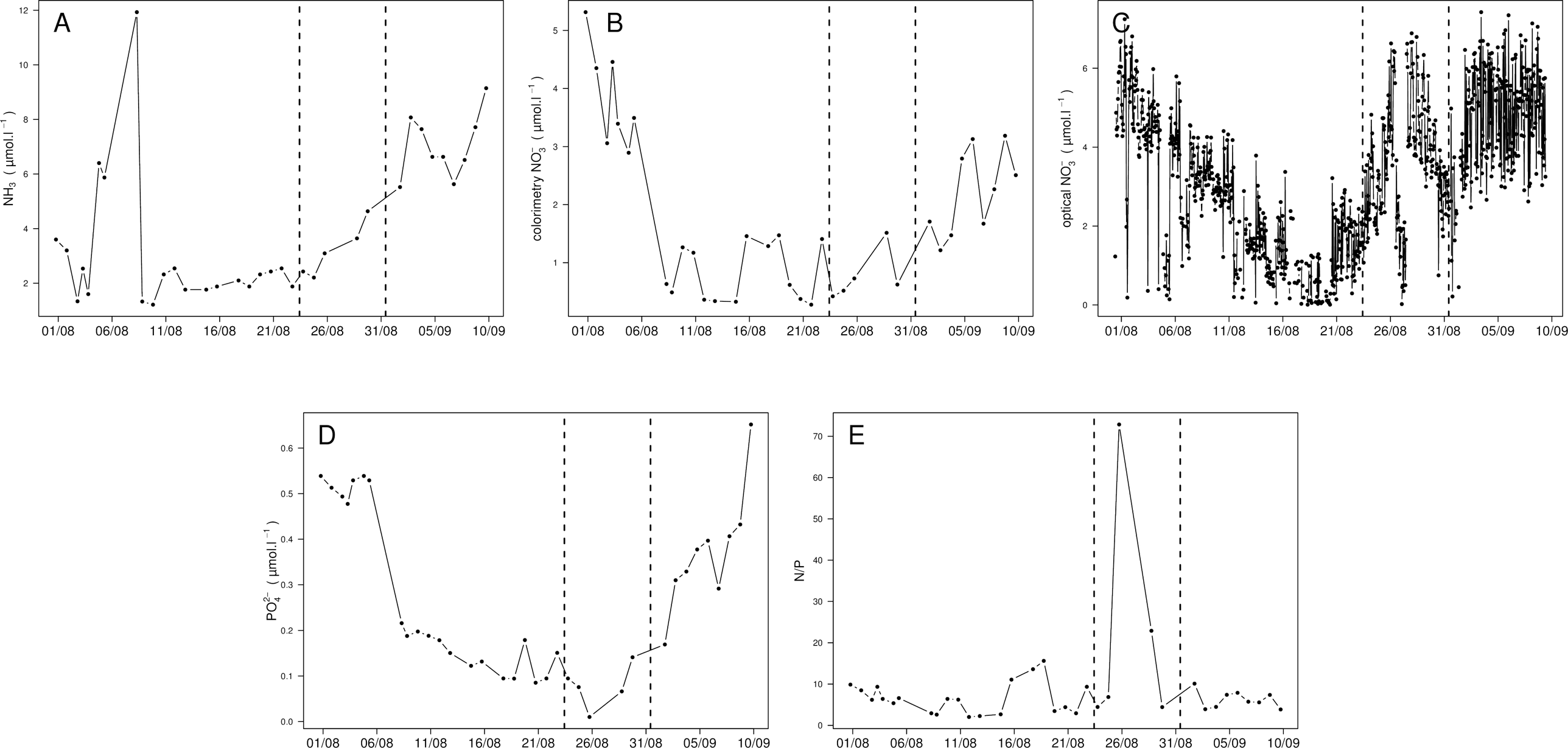
A
B
C
D
E
NH_3 (µmol.l $^{-1}$)
colorimetry NO_3^- (µmol.l $^{-1}$)
optical NO_3^- (µmol.l $^{-1}$)
PO_4^{2-} (µmol.l $^{-1}$)
N/P
01/08
06/08
11/08
16/08
21/08
26/08
31/08
05/09
10/09

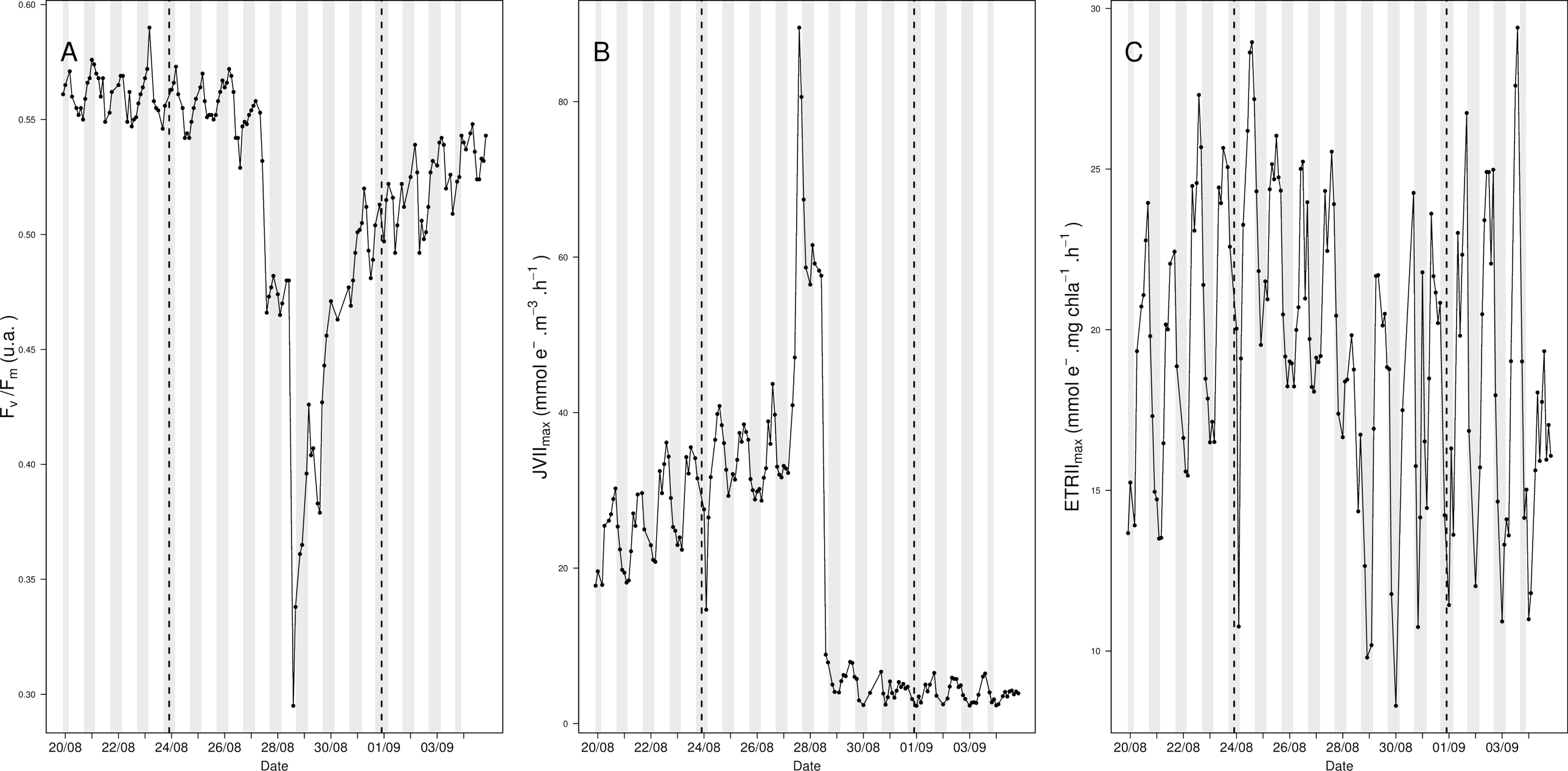
A
B
C
F_v/F_m (u.a.)
$JVII_{max}$ (mmol e^- .m^{-3} .h^{-1})
$ETRII_{max}$ (mmol e^- .mg $chla^{-1}$ .h^{-1})
0.60
0.55
0.50
0.45
0.40
0.35
0.30
80
60
40
20
0
30
25
20
15
10
20/08
22/08
24/08
26/08
28/08
30/08
01/09
03/09
Date

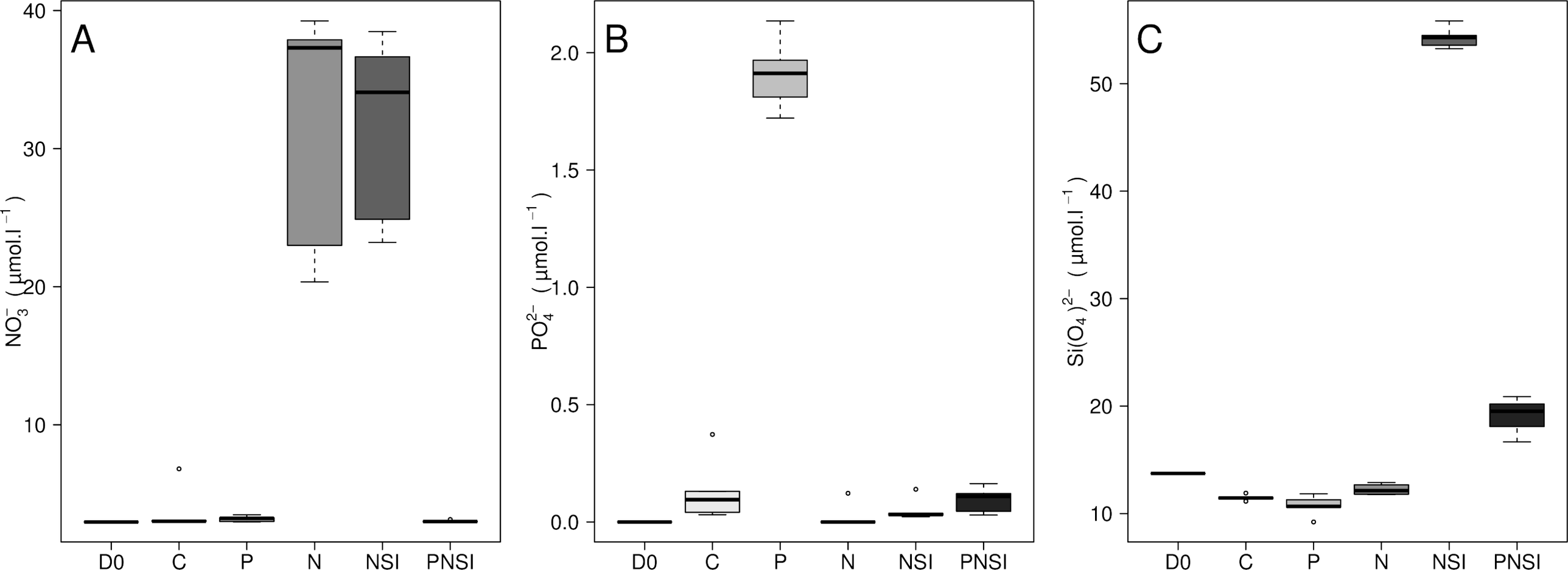
A
B
C
NO_3^- (µmol.l^{-1})
PO_4^{2-} (µmol.l^{-1})
$Si(O_4)^{2-}$ (µmol.l^{-1})
D0
C
P
N
NSI
PNSI

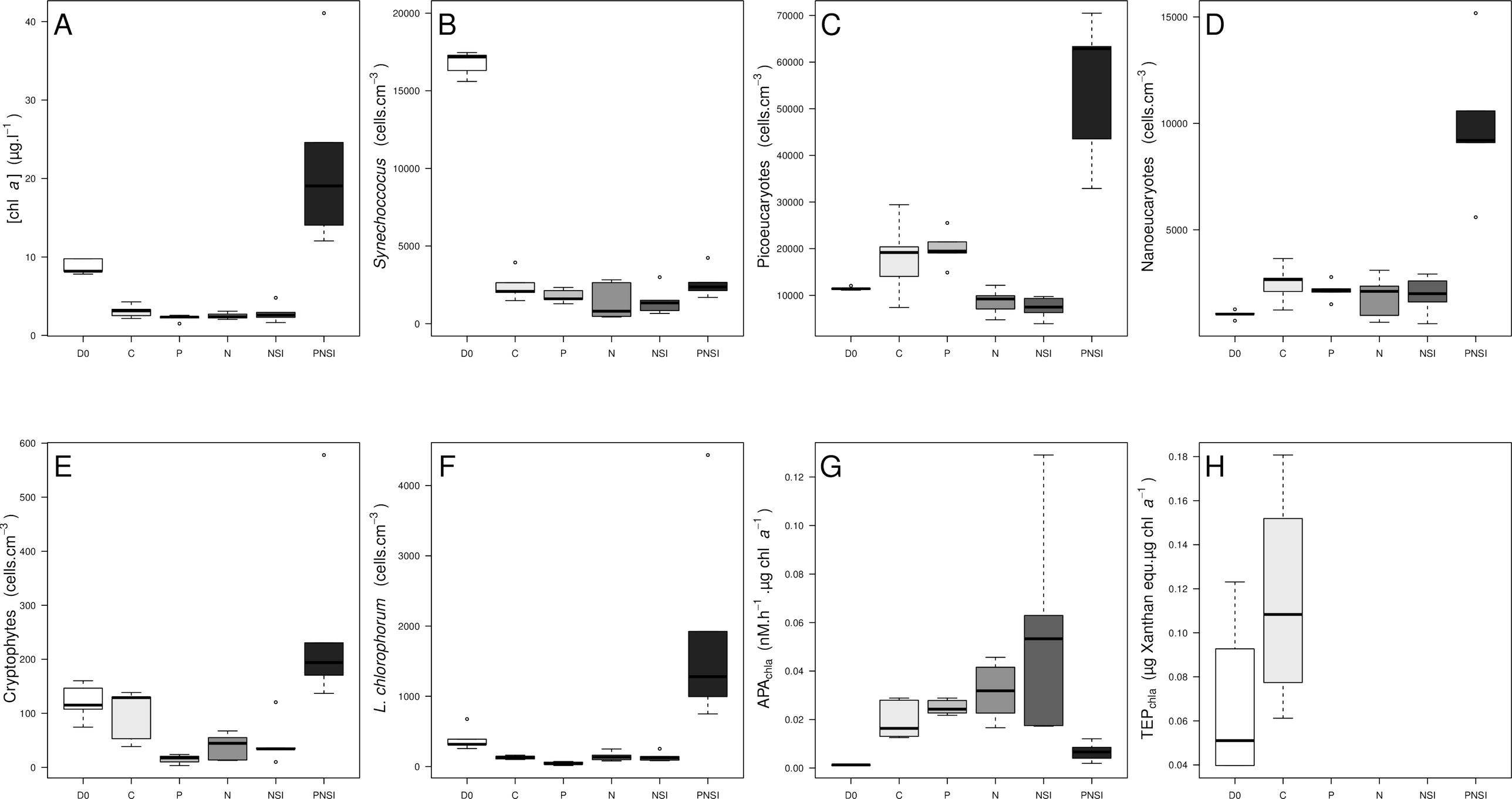
A
[chl a] (µg.l−1)
B
Synechoccocus (cells.cm−3)
C
Picoeucaryotes (cells.cm−3)
D
Nanoeucaryotes (cells.cm−3)
E
Cryptophytes (cells.cm−3)
F
L. chlorophorum (cells.cm−3)
G
APAchla (nM.h−1.µg chl a−1)
H
TEPchla (µg Xanthan equ.µg chl a−1)
D0
C
P
N
NSI
PNSI

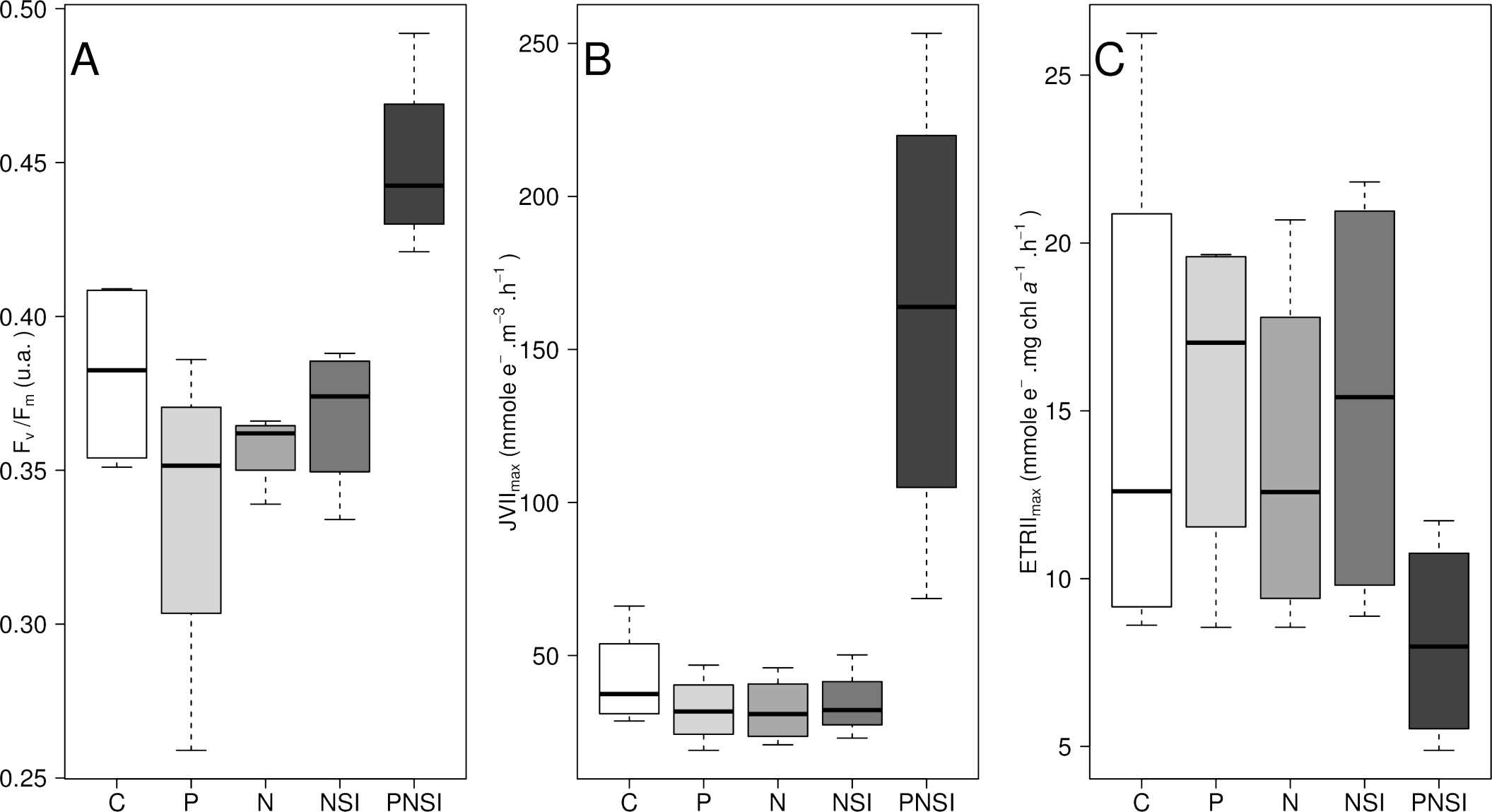
A
B
C
F_v/F_m (u.a.)
$JVII_{max}$ (mmole $e^-.m^{-3}.h^{-1}$)
$ETRII_{max}$ (mmole e^-.mg chl $a^{-1}.h^{-1}$)
0.50
0.45
0.40
0.35
0.30
0.25
250
200
150
100
50
25
20
15
10
5
C
P
N
NSI
PNSI

Bloom

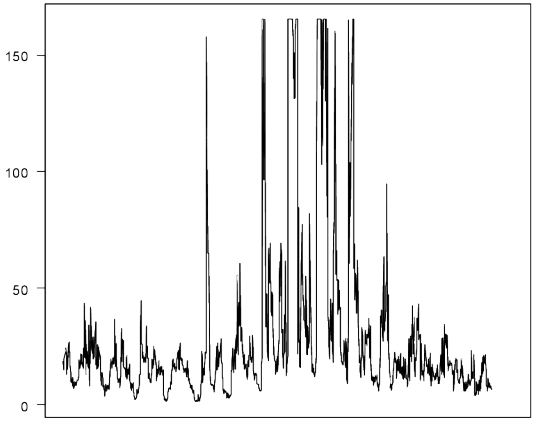

Fluorescence

Trigger

Collapse

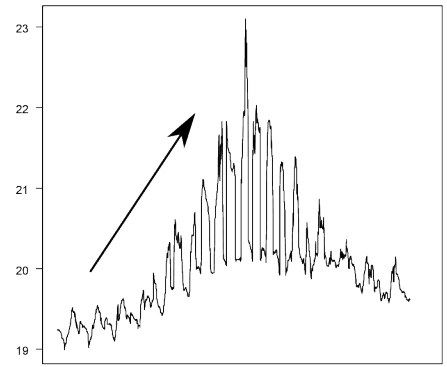

Temperature

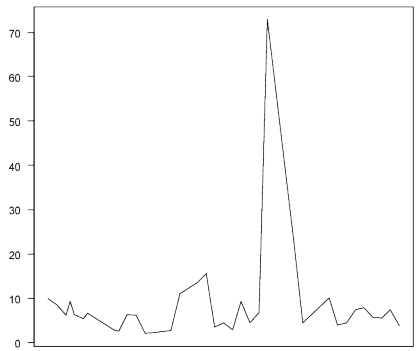

N:P

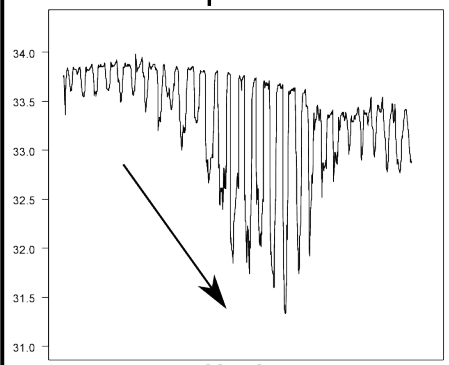

Salinity

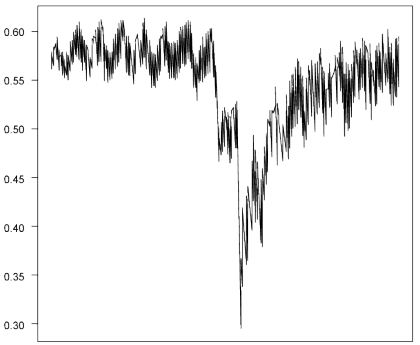

Fv/Fm

Bioassay

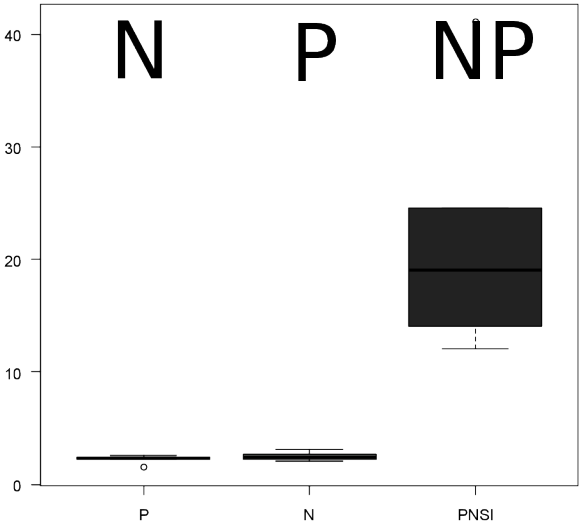

[Chla]

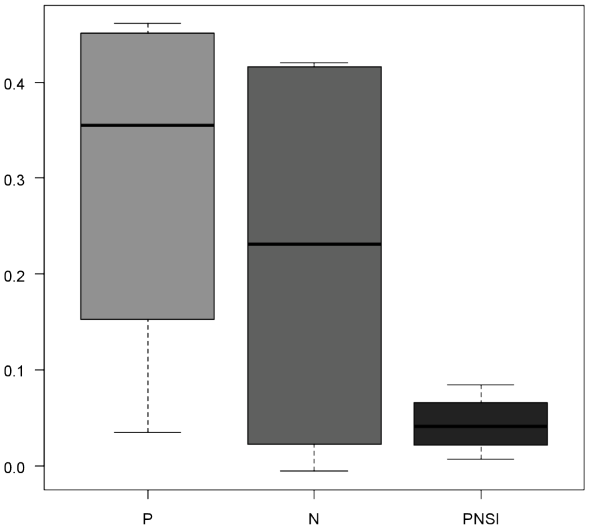

TEP